© 2013. Published by The Company of Biologists Ltd | Development (2013) 140, 4763-4775 doi:10.1242/dev.098509

RESEARCH ARTICLE

Par3 controls neural crest migration by promoting microtubule catastrophe during contact inhibition of locomotion

Rachel Moore[1], Eric Theveneau[1], Sara Pozzi[1], Paula Alexandre[2], Joanna Richardson[3], Anne Merks[4], Maddy Parsons[3], Jubin Kashef[4], Claudia Linker[3] and Roberto Mayor[1,*]

ABSTRACT

There is growing evidence that contact inhibition of locomotion (CIL) is essential for morphogenesis and its failure is thought to be responsible for cancer invasion; however, the molecular bases of this phenomenon are poorly understood. Here we investigate the role of the polarity protein Par3 in CIL during migration of the neural crest, a highly migratory mesenchymal cell type. In epithelial cells, Par3 is localised to the cell-cell adhesion complex and is important in the definition of apicobasal polarity, but the localisation and function of Par3 in mesenchymal cells are not well characterised. We show in *Xenopus* and zebrafish that Par3 is localised to the cell-cell contact in neural crest cells and is essential for CIL. We demonstrate that the dynamics of microtubules are different in different parts of the cell, with an increase in microtubule catastrophe at the collision site during CIL. Par3 loss-of-function affects neural crest migration by reducing microtubule catastrophe at the site of cell-cell contact and abrogating CIL. Furthermore, Par3 promotes microtubule catastrophe by inhibiting the Rac-GEF Trio, as double inhibition of Par3 and Trio restores microtubule catastrophe at the cell contact and rescues CIL and neural crest migration. Our results demonstrate a novel role of Par3 during neural crest migration, which is likely to be conserved in other processes that involve CIL such as cancer invasion or cell dispersion.

KEY WORDS: Par3, Pard3, Contact inhibition of locomotion, Neural crest, Microtubule catastrophe, Cell polarity, Cell migration, Trio, Rac

INTRODUCTION

Cell migration underlies numerous events during development and in adult life, controlling such diverse processes as morphogenesis, angiogenesis, axon pathfinding, wound healing, immune surveillance and metastasis. During migration, cells must determine the direction in which to migrate and reorient their cytoskeleton so as to establish protrusions at the leading edge and retraction at the trailing edge. This cell polarisation can be induced by cell-cell contact during contact inhibition of locomotion (CIL), the phenomenon by which a cell, upon contact with another cell, collapses its protrusions, reorientates and migrates in another direction (Abercrombie and Heaysman, 1953) (for reviews, see Batson et al., 2013; Stramer et al., 2013). Indeed, it has been shown that CIL plays a major role in controlling the directional migration of neural crest (NC) cells (Carmona-Fontaine et al., 2008; Matthews et al., 2008; Theveneau et al., 2010; Theveneau et al., 2013), a mesenchymal cell population with a migratory behaviour that has been likened to cancer metastasis (Theveneau and Mayor, 2011).

Polarisation by CIL is a complex process that involves several steps: cell contact, collapse of cell protrusions, formation of new protrusions away from the contact, cell separation and migration (Mayor and Carmona-Fontaine, 2010; Stramer et al., 2010). Some molecular regulators of CIL have been identified in recent years, such as small GTPases, planar cell polarity (PCP) signalling, N-cadherin and Eph-ephrins (Carmona-Fontaine et al., 2008; Kadir et al., 2011; Matthews et al., 2008; Theveneau et al., 2010), but how these molecules can control the cytoskeletal rearrangements required for a CIL response remains unknown.

Cell-cell contacts play a major role in the collective directional migration of NC in *Xenopus*, zebrafish and chick embryos (Carmona-Fontaine et al., 2008; Matthews et al., 2008), presumably because cell contact is a key step in CIL. Recent evidence indicates that, during cell contact between NC cells, a transient cell adhesion complex is formed (Theveneau et al., 2010; Theveneau et al., 2013). The formation of a cell-cell adhesion complex is unexpected, as NC cells are mesenchymal cells with reduced cell-cell adhesion (Theveneau and Mayor, 2012). In epithelial cells, the adhesion complex identifies and reinforces the boundary between apical and basolateral membranes to maintain cell polarity and tissue structure. It also serves as a signalling focal point, orchestrating various signalling events via the recruitment of regulatory factors such as the cell polarity protein Par3 (also known as Pard3) (Gao et al., 2002; Izumi et al., 1998; Kuchinke et al., 1998; Suzuki et al., 2001). However, the composition of a cell adhesion complex in mesenchymal cells, such as the NC, is poorly characterised and, more importantly, its downstream effectors remain elusive.

Par3 promotes the maturation of the cell adhesion complex and has been linked to the regulation of microtubule dynamics and Rac1 activity through interaction with the Rac-GEF Tiam1 (Chen et al., 2013; Chen and Macara, 2005; Mack et al., 2012; Mertens et al., 2005; Mishima et al., 2002; Xue et al., 2013). In epithelial cells, Par3 associates with cell-cell adhesion complexes and appears to be important for establishing apicobasal polarity; however, whether Par3 controls PCP during CIL remains to be investigated. Par3 also appears to have roles in controlling microtubule dynamics during periods of cell motility (Du et al., 2010; Nishimura et al., 2005; Pegtel et al., 2007; Schmoranzer et al., 2009; Shin et al., 2007). For example, in wound healing assays, Par3 has been found to play an important role at the leading edge of migratory cells, controlling centrosome polarisation, microtubule orientation and microtubule dynamics (Du et al., 2010; Schmoranzer et al., 2009; Shin et al., 2007). Thus, as Par3 controls microtubule dynamics, cell migration and polarity and is localised at the cell-cell junction of epithelial

[1]Department of Cell and Developmental Biology, University College London, London WC1E 6BT, UK. [2]MRC Centre for Developmental Neurobiology, King's College London, London SE1 1UL, UK. [3]Randall Division of Cell and Molecular Biophysics, King's College London, London SE1 1UL, UK. [4]Karlsruhe Institute of Technology, Zoological Institute, Cell and Developmental Biology, 76131 Karlsruhe, Germany.

*Author for correspondence (r.mayor@ucl.ac.uk)

Received 7 May 2013; Accepted 5 September 2013

Development (2013) doi:10.1242/dev.098509

cells, it represents a possible candidate to participate in CIL of mesenchymal cells.

To investigate a possible role of Par3 in CIL during collective cell migration, we turned to NC cells. We found that Par3 is required for NC migration by controlling the CIL response of these cells. Par3 is localised at cell-cell contacts between NC cells, where it interacts with the Rac-GEF Trio. We show that Par3 exerts its effect by promoting microtubule catastrophe at the cell contact and that Par3 inhibition can be rescued by concurrent inhibition of Trio. Thus, we propose that CIL requires of local destabilisation of microtubules at the cell-cell contacts, which is controlled in a Par3/Trio-dependent manner.

RESULTS

Par3 is required for NC migration

To investigate the role of Par3 in NC migration, we performed a loss-of-function experiment using an antisense morpholino (MO) against *Par3* (Par3MO), which efficiently decreases the level of Par3 protein in *Xenopus* embryos (Fig. 1A). Injection of Par3MO

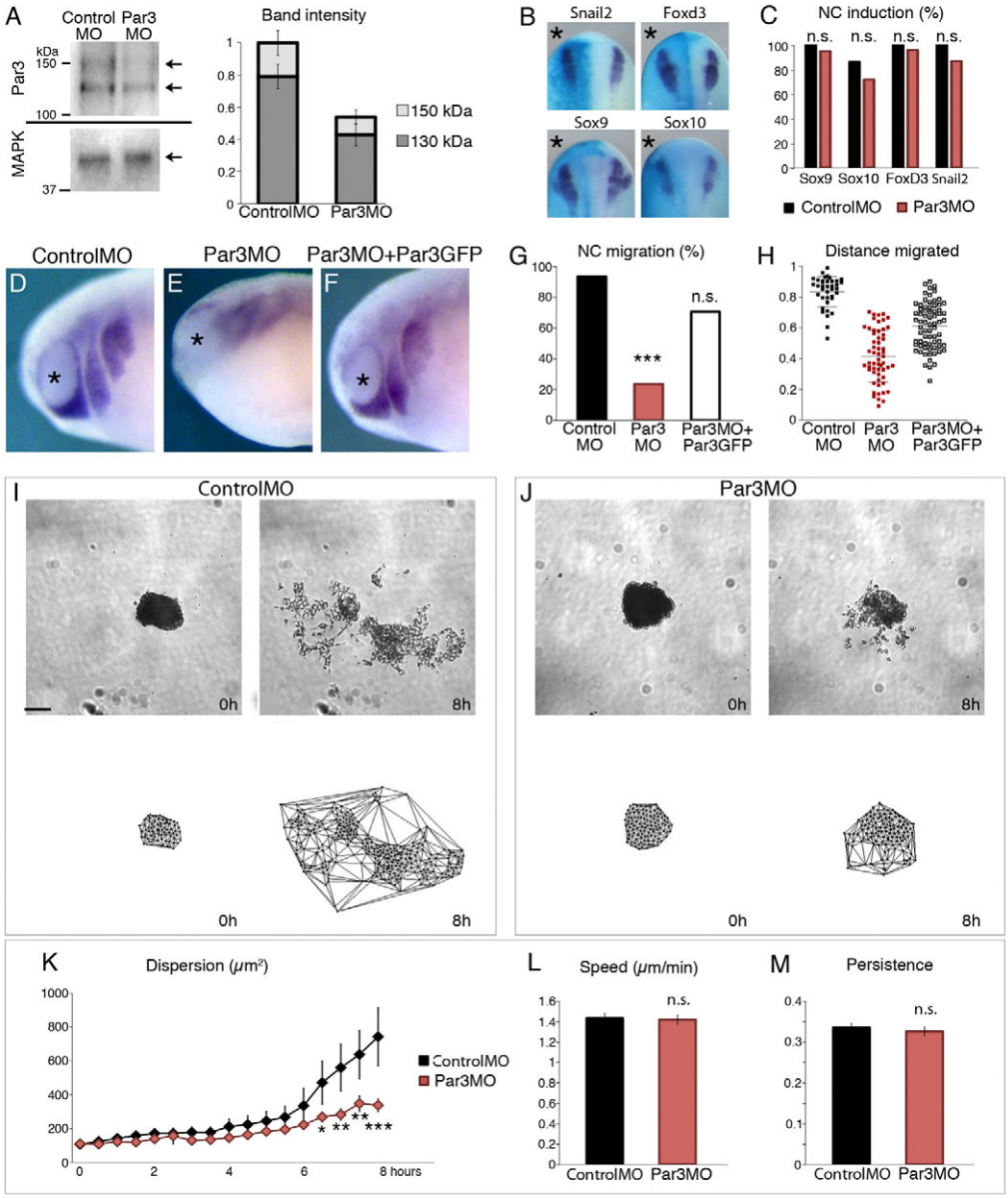

Fig. 1. Par3 is required for NC migration in *Xenopus*. (A) Western analysis of Par3 using protein extracts from *Xenopus* embryos injected with ControlMO or Par3MO. Band intensity is shown relative to ControlMO and normalised to the loading control (MAPK). Arrows indicate individual Par3 and MAPK bands. Error bars show s.d. The experiment was repeated three times; the difference between control and Par3MO was significant (P<0.005). (B) Dorsal view of stage 16 *Xenopus* embryo injected unilaterally with Par3MO (asterisk) and processed for *in situ* hybridisation against *Snail2*, *FoxD3*, *Sox9* and *Sox10*. (C) Par3MO does not affect NC induction (n=181). n.s., not significant. (D-F) Lateral view of *Xenopus* embryos showing *Twist* expression for ControlMO (D), Par3MO (E) or Par3MO co-injected with mRNA for zebrafish Par3GFP (F). Asterisk marks the eye. (G) Percentage of embryos with normal NC migration. Par3MO, n=45; ControlMO, n=24; P<0.001; Par3MO+Par3GFP, n=34; P<0.001. (H) Distance migrated by NC cells relative to mean migration in control embryos. Migration is reduced in Par3MO-injected embryos (P<0.001) but co-injection of Par3GFP with Par3MO rescues migration (P<0.001). (I,J) Single frames from time-lapse movies showing control (I) and Par3MO-injected (J) explants and Delaunay triangulation at 0 and 8 hours. Scale bar: 100 μm. (K) Dispersion between cells increases over time in control but not in Par3MO-injected explants (n=8 explants for each condition, more than 30 cells analysed per explant; *P<0.05, **P<0.01, ***P<0.001). (L) Speed of single NC cells. n=20 per experiment, from three independent experiments; P=0.2146. (M) Persistence of single NC cells. n=20 experiment, from three independent experiments; P=0.4021. (K-M) Error bars indicate s.d.

Development (2013) doi:10.1242/dev.098509

did not affect NC induction, as analysed by *in situ* hybridisation against *Snail2*, *FoxD3*, *Sox9* or *Sox10*, all of which are known markers for pre-migratory NC (Fig. 1B,C). However, Par3MO injection had a dramatic effect on NC migration, as analysed by *in situ* hybridisation against *Twist*, which marks migrating NC (Fig. 1D,E,G). Importantly, this effect can be rescued by co-injection of zebrafish *par3* mRNA, which does not contain the sequence targeted by the MO against *Xenopus Par3* (Fig. 1F-H), demonstrating specificity for the Par3MO. The requirement of Par3 is cell-autonomous, as grafts of Par3-depleted cells into normal host show a clear defect in NC migration (supplementary material Fig. S1).

To further assess the necessity for Par3 in NC migration, NC explants were cultured on fibronectin and observed by time-lapse imaging. Control explants tended to disperse after a few hours of cell culture (Fig. 1I), as previously described (Alfandari et al., 2003), whereas explants injected with Par3MO failed to disperse (Fig. 1J; supplementary material Movie 1). We quantified cell dispersion by measuring the area of the triangles formed between the nuclei using Delaunay triangulation as previously described (Carmona-Fontaine et al., 2011). A dramatic increase in cell dispersion starts at ~6 hours in the control explants, but this is very much reduced in Par3MO-injected explants (Fig. 1K). This reduced dispersion is not due to an effect on cell motility, as control and Par3MO-injected cells exhibited similar speeds and persistence during the migration of individual cells (Fig. 1L,M). These results demonstrate that Par3 is not required for cell motility but is required for NC dispersion.

Our results show an effect of Par3MO on *Xenopus* NC migration *in vivo* and *in vitro*. Next, we turned to zebrafish embryos to perform live imaging of NC migration, as it is easier to obtain high-resolution images in zebrafish than in *Xenopus* for quantitative analysis *in vivo*. First, we confirmed that a similar NC phenotype was achieved using a previously characterised zebrafish Par3MO (Wei et al., 2004). Indeed, injection of Par3MO leads to a clear inhibition of migration in trunk (Fig. 2B-D) and cephalic (Fig. 2B,E,F) NC cells, without affecting NC induction (Fig. 2A). To analyse cell behaviour *in vivo*, a new transgenic zebrafish line that

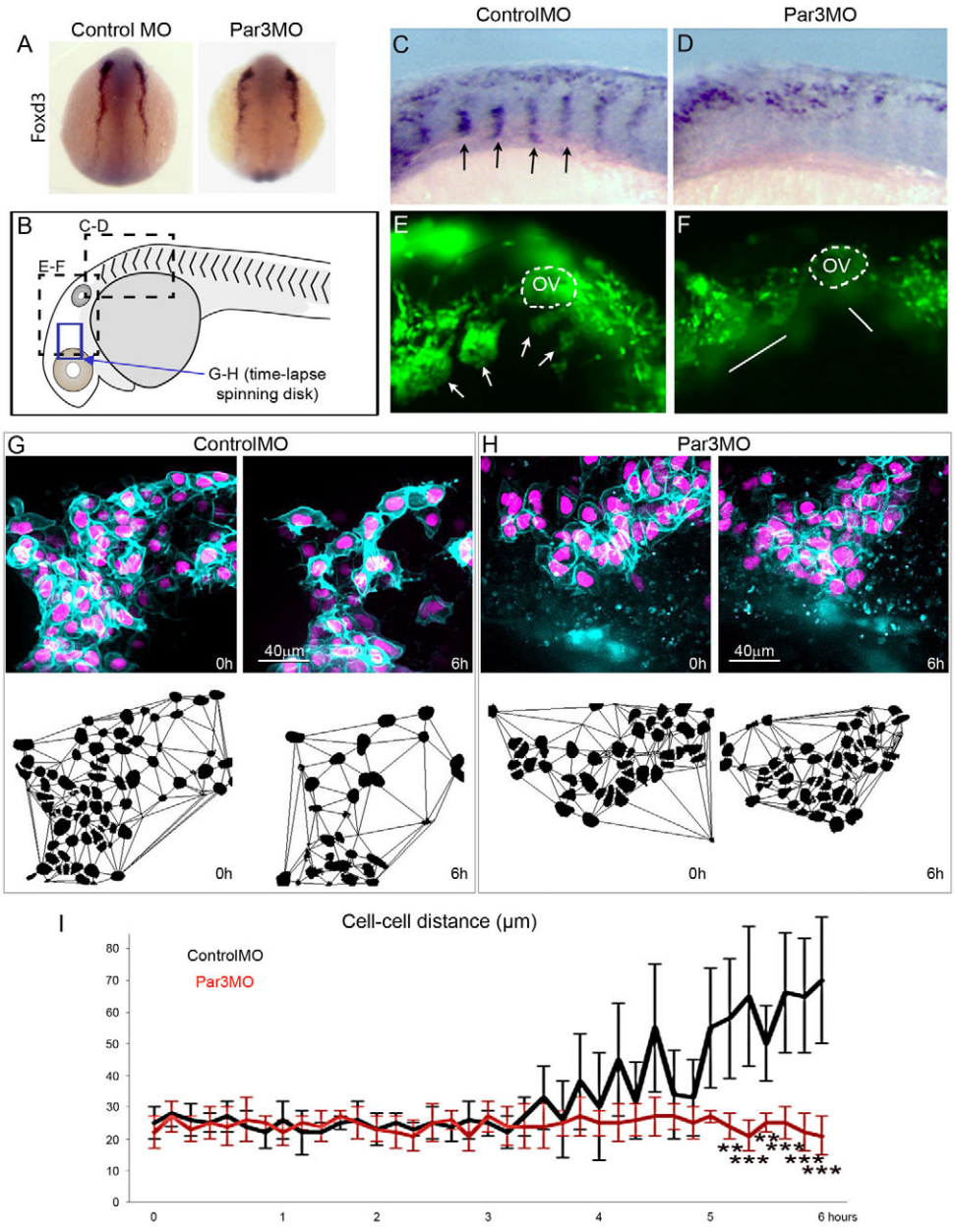

Fig. 2. Par3 is required for NC migration in zebrafish. (A) Dorsal view of 5-somite stage zebrafish embryos injected unilaterally with ControlMO or Par3MO and processed for *in situ* hybridisation against *foxd3*; no effect on NC induction was observed (n=72). (B) Schematic representation of zebrafish embryo indicating the regions shown in C-H. (C,D) Lateral views showing *foxd3* expression in the trunk of ControlMO-injected (C) or Par3MO-injected (D) 20-somite embryos. Arrows indicate distinct trunk NC streams. (E,F) Lateral views showing heads of 24-hour *sox10:egfp* embryos injected with ControlMO (E) or Par3MO (F). OV, otic vesicle. Arrows indicate distinct cranial NC streams. Lines indicate that no distinct streams are observed. (G,H) Single frames from time-lapse movies showing one cranial NC stream and corresponding Delaunay triangulation at 0 hours (15 somites) and 6 hours from ControlMO-injected (G) and Par3MO-injected (H) embryos. (I) Distance between cranial NC cells analysed by nearest neighbour computation. n=15 embryos for each condition, with more than 30 cells analysed per explant; $^{**}P<0.01$, $^{***}P<0.001$. Error bars indicate s.d.

Development (2013) doi:10.1242/dev.098509

expresses membrane-GFP and nuclear-RFP under the NC-specific *Sox10* promoter was developed. Similar to the *in vitro* observation using *Xenopus* NC, Par3MO reduced NC dispersion *in vivo* (Fig. 2G-I; supplementary material Movie 2).

One way in which Par3 could affect dispersion is through controlling cell-cell adhesion, as has been shown in other cell types (Chen and Macara, 2005; Mertens et al., 2005; Mishima et al., 2002). We analysed the effect of Par3MO on the level and localisation of various cell adhesion proteins. No effect was found on the localisation of β-catenin or p120-catenin (also known as δ1 catenin) at the cell-cell junction in Par3MO-injected cells compared with control *Xenopus* NC cells (Fig. 3A-F), nor in the level or localisation of N-cadherin between control or Par3MO-injected cells in zebrafish embryos (Fig. 3G-L). Furthermore, we performed a cell-sorting assay to evaluate whether Par3MO influenced cell-cell adhesion (Fig. 3M). When control and N-cadherin morphant cells are mixed they sort out, indicating differential cell adhesion (Fig. 3P) (Friedlander et al., 1989). However, when control and Par3MO-injected cells are combined, a mixed cell population results with no difference between control and Par3 morphant cells (Fig. 3N,O). Together, our results did not support a role for Par3 in regulating cell adhesion between NC cells, and an alternative mechanism for the effect of Par3 inhibition on NC migration and dispersion needed to be explored.

Par3 is required for CIL

An alternative way in which Par3 could affect NC dispersion is through controlling CIL, as CIL promotes dispersion by repolarising the cells away from each other upon cell contact (Mayor and Carmona-Fontaine, 2010). We performed three different assays that have been used previously to analyse CIL (Abercrombie and Heaysman, 1953; Carmona-Fontaine et al., 2008; Theveneau et al., 2010). First, two NC explants confronted with each other do not overlap if they exhibit CIL (Fig. 4A). Par3MO-injected explants widely overlapped, as did pairs comprising one control and one Par3MO-injected explant, indicating a failure in CIL (Fig. 4A-D). Second, CIL dictates that two adjacent cells do not make protrusions on top of one another (Fig. 4E) (Abercrombie and Heaysman, 1953); however, Par3MO-injected NC cells extended protrusions on top of their neighbours (Fig. 4F,G; supplementary material Movie 3). Third, the hallmark of CIL is that collision between two single cells will cause them to change velocity if CIL occurs (Fig. 4H) (Abercrombie and Heaysman, 1953). However, colliding Par3MO-injected cells showed a significantly reduced change in velocity upon collision compared with control cells (Fig. 4I,J; supplementary material Movie 4). Together, these results indicate that Par3 is required for CIL between NC cells in *Xenopus* embryos. Next, we used the *sox10:mGFPnRFP* zebrafish line to analyse CIL *in vivo*. Collisions between NC cells were analysed after time-lapse imaging of migrating NC. ControlMO-injected NC cells exhibited the typical CIL response by changing the direction of migration after collision (Fig. 5A-C; supplementary material Movie 5). By contrast, Par3MO-injected NC cells failed to change the direction of migration after colliding with another NC cell (Fig. 5D-F; supplementary material Movie 6). These experiments confirm that Par3 is required for CIL between NC cells *in vitro* and *in vivo*.

To determine the precise role of Par3 during CIL, it was important to assess Par3 localisation. To analyse the dynamics of Par3 localisation, embryos were injected with Par3GFP mRNA and time-lapse imaging was performed on cultured NC. Par3GFP localised to

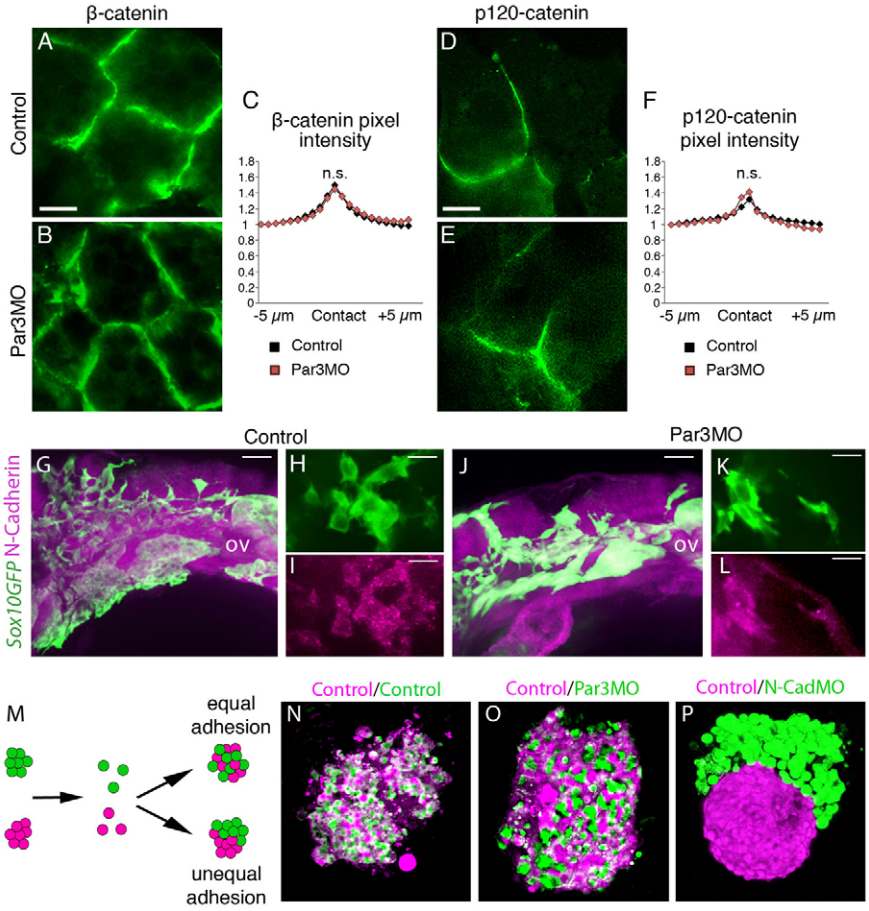

Fig. 3. Par3 inhibition does not affect cell adhesion in *Xenopus* or zebrafish. (A-F) Cell adhesion molecules analysed in *Xenopus* embryos. (A-C) Immunostaining against β-catenin in control (A) or Par3MO-injected NC cells (B). (C) Pixel intensity of β-catenin immunostaining was measured across the contact and normalised to the average value background levels 5 μm away from the contact for each image. There is no difference in pixel intensity between control cells (n=84 contacts) and Par3MO-injected cells (n=44 contacts; P>0.05 at all distances from contact). (D-F) Control (D) or Par3MO-injected (E) NC cells expressing p120-cateninGFP. (F) Pixel intensity analysis as described in C. There is no difference in pixel intensity of p120-catenin immunostaining between control cells (n=24 contacts) and Par3MO-injected cells (n=41 contacts; P>0.05 at all distances from contact). (G-L) N-cadherin immunostaining in control (G-I) or Par3MO injected (J-L) zebrafish embryos. *sox10GFP* transgenic embryos were used to identify NC cells. Note that N-cadherin staining is not affected by Par3MO in the NC. n=150 embryos, fixed at 24 hpf. (M-P) Cell adhesion is not affected by Par3MO. (M) Schematic representation of the cell reaggregation assay. (N) Control *Xenopus* NC cells. (O) Control/Par3MO *Xenopus* NC cells. (P) Control/N-cadherinMO *Xenopus* NC cells. Scale bars: 10 μm.

Development (2013) doi:10.1242/dev.098509

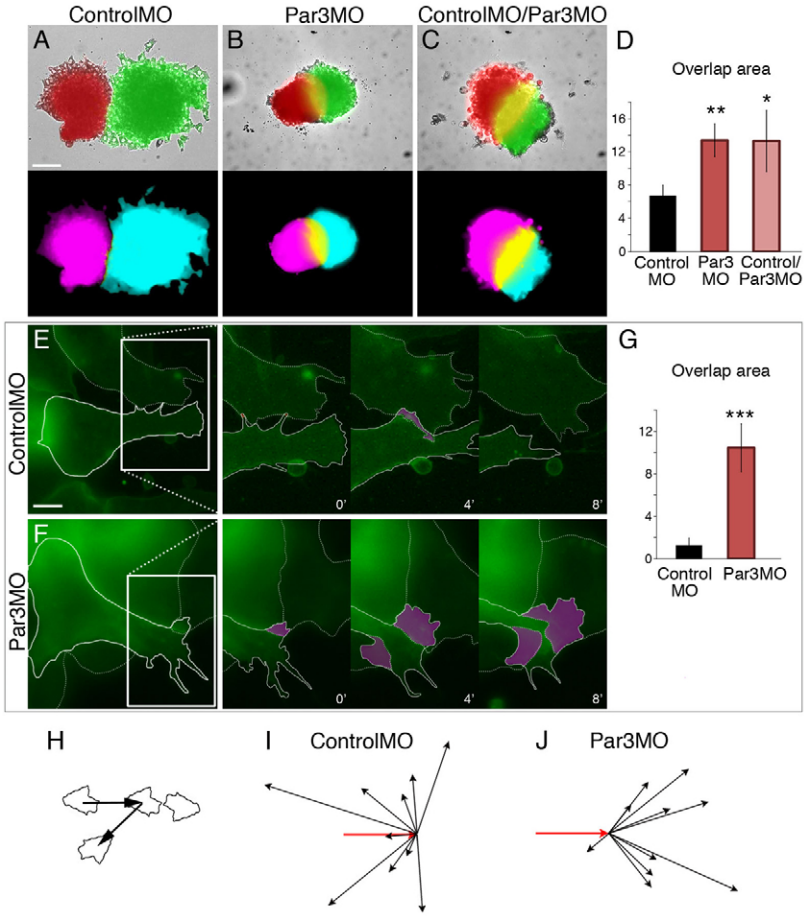

Fig. 4. Par3 is required for CIL *in vitro* in *Xenopus*. (A-D) Explant confrontation assay. (A-C) Single frames from time-lapse movies showing maximum overlap between two control explants (A), two Par3MO-injected explants (B) or one control and one Par3MO-injected explant (C). (D) Overlap area as a percentage of total explant area. Control/control, n=27; Par3MO/Par3MO, n=16; P=0.0026; control/Par3MO, n=9; P=0.0252. (E-G) Protrusions overlap analysis for ControlMO-injected (E) or Par3MO-injected (F) cells expressing mbGFP. Magenta overlay shows the protrusion overlap. (G) Protrusion overlap area as a percentage of cell area. Par3MO, n=40; control, n=50; P=0.0002. (H-J) Cell collision assay. (H) Schematic representation of cell collision. Cell position was analysed at 15-minute intervals to measure velocity following collision between ControlMO-injected (I) or Par3MO-injected (J) cells. Velocity vectors were clustered away from the contact in control cells (n=10; P<0.001) but a change in velocity following collision was not observed in Par3MO-injected cells (n=10; P<0.001). Red arrows indicate the initial velocity vector. *P<0.05, **P<0.01, ***P<0.001. Error bars indicate s.d. Scale bars: 100 μm in A; 10 μm in E.

cell junctions both in clusters of NC cells that were already in contact (Fig. 6A) and during collisions between individual cells (Fig. 6B; supplementary material Movie 7). To confirm that endogenous Par3 was expressed in *Xenopus* NC and localised to cell-cell contacts, membraneRFP (mbRFP)-labelled NC cells were transplanted into wild-type host embryos to identify the migrating NC and immunostaining against Par3 was performed. Our results showed that endogenous Par3 was present in the NC and colocalised with mbRFP at cell-cell contacts (Fig. 6C-F).

Par3 promotes microtubule catastrophe at cell-cell contacts

How does Par3 regulate CIL in NC cells? Par3 has been shown to control microtubule array polarisation in other cell types by affecting microtubule dynamics or centrosome positioning (Pegtel et al., 2007; Schmoranzer et al., 2009). Furthermore, microtubules are involved in CIL (Kadir et al., 2011; Stramer et al., 2010). Thus, we next investigated a possible interaction between Par3 and microtubules as a means of regulating CIL. However, Par3 inhibition had no effect on the entire microtubule array (Fig. 6G,H), nor on a stable microtubule subpopulation containing acetylated tubulin (Fig. 6I,J).

To analyse microtubule dynamics we labelled NC cells with EB3GFP and performing time-lapse imaging, which allows high-resolution visualisation of growing microtubules (supplementary material Movie 8). We tracked EB3GFP comets and compared the number of microtubules undergoing catastrophe (disappearing comets) with the total number of microtubules (comets) at the cell contact and at the free edge. In control cells, a greater percentage of microtubules experienced catastrophe at the contact (Fig. 7A) compared with the free edge (Fig. 7C). However, inhibiting Par3 abolished the increase in microtubule catastrophe at the contact (Fig. 7B,C; supplementary material Movie 9). This suggests that Par3 is required at the cell-cell contacts to promote microtubule catastrophe.

A caveat of using EB3GFP-labelled cells is that collapsing and pausing microtubules are not easy to distinguish or quantify manually. Therefore, we used the automatic tracking software plusTipTracker (Applegate et al., 2011) to perform an exhaustive analysis of microtubule dynamics. Importantly, it calculates which tracks belong to the same microtubule, which may be cycling between phases of growth, pause and catastrophe (Applegate et al., 2011). Movies of EB3GFP-labelled cells were analysed at cell-cell contacts during collisions of *Xenopus* NC cells. Microtubule tracks were classified as being slow or fast and as short-lived or long-lived based on the mean growth speed (26 μm/minute) and mean lifetime (20 seconds) of the data set. Par3 inhibition reduced the proportion of slow, short-lived microtubules in favour of slow, long-lived microtubules (Fig. 7D-F). This suggests that slow microtubules live longer in Par3MO cells, which implies that they must be undergoing catastrophe less frequently. Indeed, statistical analysis revealed that Par3MO injection decreased the rate of microtubule catastrophe (Fig. 7G), whereas no effect of Par3 inhibition could be found on other parameters routinely used for measuring microtubule dynamics, including growth rate, depolymerisation rate, rescue rate or pause duration (Fig. 7H-K). Overall, our analysis indicates that Par3 promotes microtubule catastrophe at the cell contact during CIL.

Par3 promotion of microtubule catastrophe at the cell-cell contact could control CIL by initiating a change in cell polarity. To test whether the effect of Par3 on CIL was dependent on microtubule

Development (2013) doi:10.1242/dev.098509

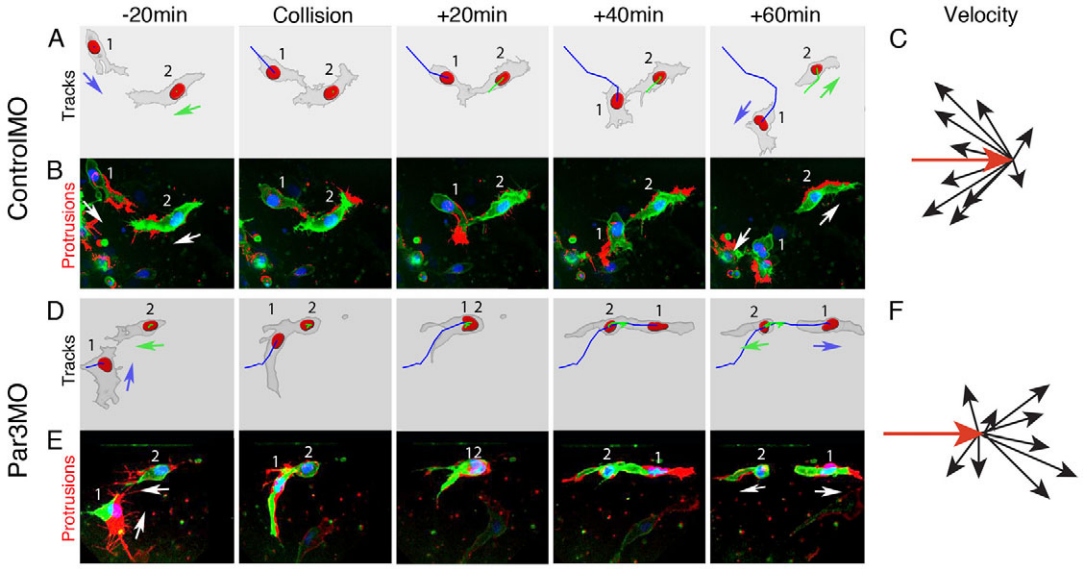

Fig. 5. Par3 is required for CIL *in vivo* in zebrafish. Single frames from time-lapse movies illustrating a collision between two cranial NC cells (1 and 2) in a zebrafish embryo injected with ControlMO (A,B) or Par3MO (D,E). Images are overlapped with tracks of migratory paths (A,D) or the difference in protrusion between current and previous frames (B,E). Red area indicates new protrusions. (C,F) Velocity vectors of colliding NC cells in ControlMO-injected (C) or Par3MO-injected (F) embryos. Cell position was recorded at 5-minute intervals. Velocity change was clustered in ControlMO-injected cells (n=10; P<0.05), but no difference in the velocity change was observed in Par3MO-injected cells (n=9; P>0.1). Red arrow indicates the initial velocity vector.

catastrophe, we attempted to rescue the Par3 morphant phenotype using a mild concentration of nocodazole (13 nM), which has a partial effect on microtubule depolymerisation (supplementary material Fig. S2) and has no effect on NC dispersion (supplementary material Fig. S3). As described above, Par3MO blocks NC dispersion; however, treatment of Par3MO-injected cells with a mild concentration of nocodazole was able to rescue cell dispersion (Fig. 8A, compare black and blue curves; supplementary material Movie 10), in spite of a small reduction in the motility of Par3MO-injected cells (Fig. 8B,C, blue bars). On control cells, nocodazole inhibited CIL (not shown). Importantly, the explant confrontation assay showed that the increased overlap area induced by Par3MO (Fig. 8D,E,H) was reduced by nocodazole treatment (Fig. 8F,H, blue bar), indicating that CIL behaviour was restored. Furthermore, analysis of CIL in single cell collisions showed that the loss of CIL in Par3MO-injected cells (Fig. 8I,J) was rescued by nocodazole treatment (Fig. 8K; supplementary material Movie 11). This supports the notion that Par3 controls CIL by promoting microtubule collapse at the cell-cell contact.

Par3 interacts with Trio to promote microtubule catastrophe

It is known that Rac1 can influence cell polarity by stabilising microtubules (Pegtel et al., 2007; Wittmann et al., 2003). Thus, inhibition of Rac1 activity is a potential mechanism through which Par3 could affect microtubules. Indeed, a low concentration of the

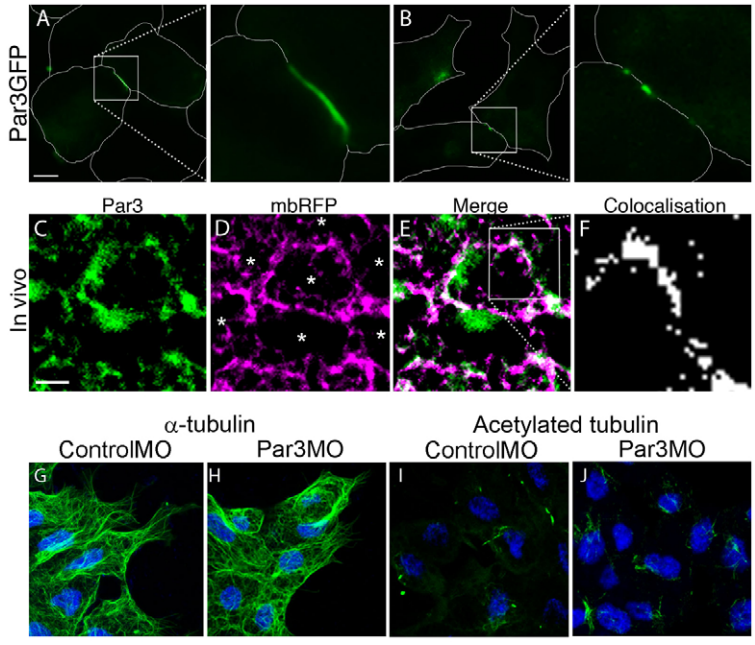

Fig. 6. Par3 is localised at the contact site of *Xenopus* NC cells and does not affect stable microtubules. (A-F) Par3GFP localises to contacts between NC cells in clusters (A) and between colliding single cells (B). (C-F) *z*-projection of confocal images showing immunostaining against endogenous Par3 in cryosections of *Xenopus* embryos. (C) Par3 is located at contacts between NC cells. (D) mbRFP identifies NC cells and cell contacts; each asterisk indicates a different cell. (E) Merge of I and J. (F) Colocalisation mask of I and J. (G-J) Analysis of microtubules in NC cells. (G,H) Immunostaining against α-tubulin shows the microtubule array in ControlMO-injected (G) and Par3MO-injected (H) cells. (I,J) Immunostaining against acetylated tubulin stains a stable subpopulation of microtubules in ControlMO-injected (I) and Par3MO-injected (J) cells. Scale bars: 10 μm in A; 20 μm in C.

Development (2013) doi:10.1242/dev.098509

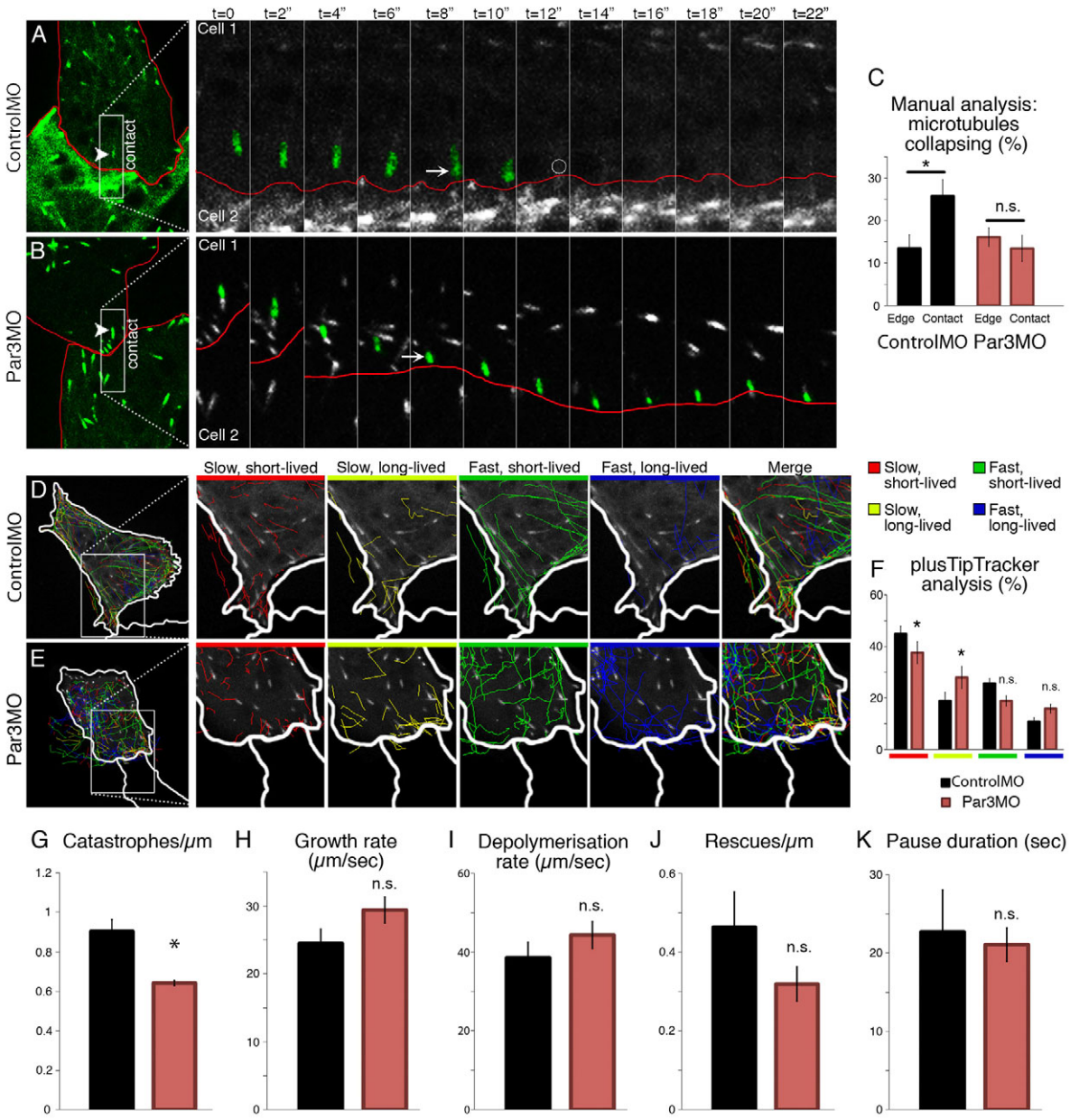

Fig. 7. Par3 affects microtubule dynamics at the cell-cell contact in *Xenopus*. (A-C) EB3GFP-labelled cells were used to analyse microtubule catastrophe. (A,B) ControlMO-injected (A) and Par3MO-injected (B) cells undergoing collision; consecutive frames are presented from time-lapse movies showing one microtubule (time is given in seconds). The boxed area is shown at higher magnification at the cell-cell contact. Arrowhead indicates the highlighted microtubule. Arrow indicates microtubule in contact with the membrane. Circle indicates site of microtubule collapse. (C) Summary of microtubule collapse at the free edge or cell contact. Control cells: n=150 from six independent experiments; *P=0.0167. Par3MO-injected cells: n=100, from six independent experiments; P=0.3. (D-K) plusTipTracker analysis of microtubules at cell-cell contacts. (D-F) Microtubule tracks in ControlMO-injected (D) and Par3MO-injected (E) cells were separated into four groups based on growth speed (slow <26 μm/minute <fast) and lifetime (short-lived <20 seconds <long-lived). (F) Par3MO-injected cells have a smaller percentage of slow, short-lived microtubules at the contact than control cells (*P=0.0276) and a greater percentage of slow, long-lived microtubules (*P=0.0238). (G-K) No difference was found between ControlMO-injected and Par3MO-injected cells in terms of growth rate (H; P>0.05), depolymerisation rate (I; P>0.05), rescue rate (J; P>0.05) or pause duration (K; P>0.05). However, Par3MO-injected cells exhibited a lower catastrophe rate at the contact compared with control cells (G; *P=0.035). A minimum of ten cells and 25 microtubules per cell were analysed from three independent experiments. Error bars indicate s.d.

Rac1 inhibitor NSC23766 was able to rescue the inhibition of cell dispersion induced by Par3MO in NC explants (Fig. 8B,C, yellow curve) without affecting the speed or persistence of migration (Fig. 8B,C, yellow bars; supplementary material Movie 10). Importantly, NSC23766 was also able to rescue CIL between Par3MO-injected explants (Fig. 8G,H, yellow bar) and between Par3MO-injected colliding cells (Fig. 8L; supplementary material Movie 11).

As Rac1 inhibition can rescue CIL in Par3MO-injected NC cells, Par3 might inhibit Rac1 during CIL. In other cell types, Par3 interacts with Rac-GEFs to influence Rac1 activity (Pegtel et al., 2007). It has been shown that the Rac-GEF Trio is an important regulator of NC migration (Kashef et al., 2009) and is therefore a possible candidate to be regulated by Par3. Indeed, we found that Par3 and Trio co-immunoprecipitate (Fig. 9A) and colocalise at NC

Development (2013) doi:10.1242/dev.098509

cell contacts (Fig. 9B-E). We next investigated whether inhibiting Trio could rescue Par3 morphant phenotypes. We developed an antisense MO against *Trio* (TrioMO) that efficiently reduced GFP fluorescence when co-injected with Trio-GFP (supplementary material Fig. S4); its NC migration phenotype can be rescued by human *TRIO*, which does not hybridise with TrioMO (supplementary material Fig. S5), demonstrating the specificity of TrioMO. We co-injected TrioMO with Par3MO to perform a double loss-of-function experiment. Trio inhibition rescued the Par3 morphant phenotype by promoting explant dispersion (Fig. 9F; supplementary material Fig. S6) without affecting the speed or persistence of migration (Fig. 9G,H; supplementary material Movie 12). Co-injection of TrioMO also rescued Par3MO-induced CIL deficiency, as analysed by the change in velocity after single cell collisions (Fig. 9I-K; supplementary material Movie 13). Finally, we analysed whether inhibition of NC migration by Par3MO *in vivo* could be rescued by inhibiting Trio. Co-injection of TrioMO with Par3MO efficiently restored NC migration *in vivo* (Fig. 9L-P). TrioMO rescue of the Par3 morphant phenotype demonstrates that Par3 inhibits Trio in NC cells.

As Rac1 has been shown to stabilise microtubules (Wittmann et al., 2003), Trio activation of Rac1 could promote microtubule stability. Thus, Par3 could promote microtubule catastrophe by inhibiting the Rac-GEF Trio. We analysed microtubule dynamics by performing time-lapse imaging of EB3GFP-labelled NC cells. Trio inhibition increased microtubule catastrophe in Par3MO-injected cells at the cell-cell contact to a level comparable to that of control cells (Fig. 10A-D). These results were supported by plusTipTracker analysis, which showed that inhibition of both Trio and Par3 increased the microtubule catastrophe rate to control levels (Fig. 10E). Finally, we measured Rac1 activity at the cell contact by fluorescence resonance energy transfer (FRET) analysis (Matthews et al., 2008). As shown previously (Theveneau et al., 2010), Rac1 activity is reduced at the cell contact in NC (Fig. 10F, control). However, inhibition of Par3 leads to a significant increase in Rac1 activity at the cell-cell interface, which is lost upon co-inhibition of Par3 and Trio (Fig. 10F,G). This supports the notion that Par3 is required at contacts between NC cells to inhibit Trio-dependent activation of Rac1, thus inhibiting Rac1-dependent microtubule stabilisation.

Altogether, our results demonstrate that Par3 controls cell protrusion collapse and reversal of cell polarity during CIL by promoting microtubule catastrophe via inhibition of the Rac-GEF Trio.

DISCUSSION

Effective NC migration is dependent on CIL. Here, we show that Par3 is required for NC migration, as it controls CIL both *in vivo* and *in vitro*. We demonstrate that Par3 controls CIL by inhibiting the Rac-GEF Trio to prevent Trio-mediated activation of Rac1 at cell-cell contacts. We propose the following model for the migration of NC cells (Fig. 11). In individually migrating cells, microtubule stability in the lamellipodia is promoted by Rac1, which is activated by Trio (Fig. 11B). Upon collision with another NC cell, Par3 is recruited to the cell-cell contact, sequestering Trio and preventing it

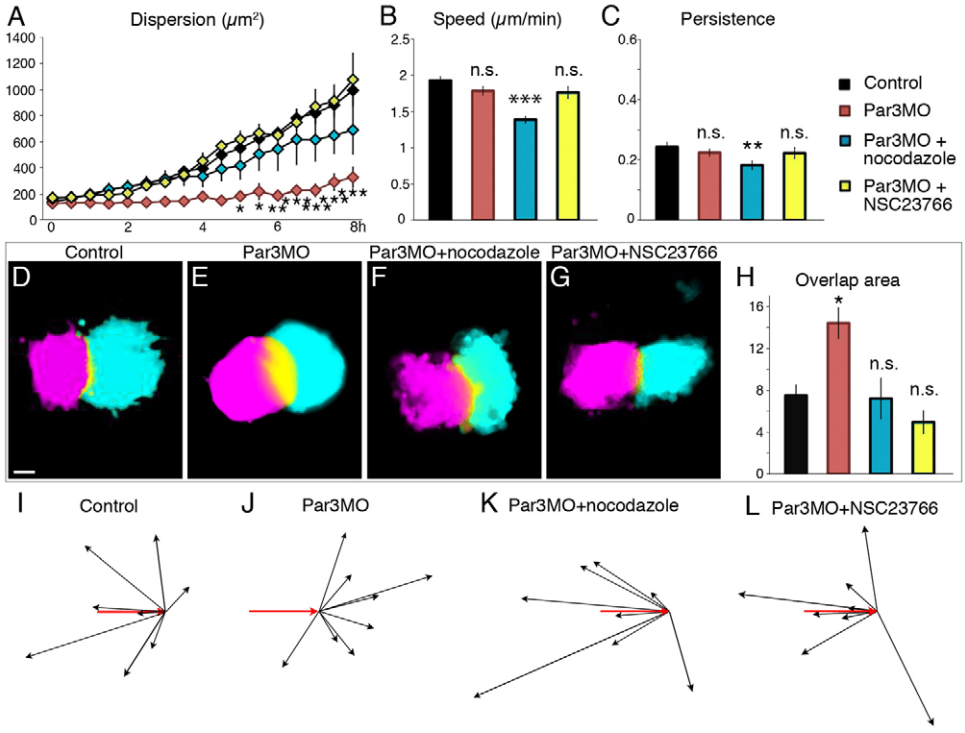

Fig. 8. The Par3 morphant phenotype is rescued with nocodazole or NSC23766 in *Xenopus*. (A) Dispersion between cells over time under the following treatments: control, Par3MO, Par3MO/nocodazole, Par3MO/NSC23766. n=10 explants for each condition, more than 30 cells analysed per explant; *P<0.05, **P<0.01, ***P<0.001. (B) Speed of cell migration. Control, n=110; Par3MO, n=120; P=0.0503; Par3MO/nocodazole, n=70; ***P=3.751x10^{-11}; Par3MP/NSC23766, n=50; P=0.0660. (C) Persistence. Control, n=100; Par3MO, n=120; P=0.3131; Par3MO/NSC23766, n=50; P=0.7696; Par3MO/nocodazole, n=70; **P=0.0064. (D-H) Explant confrontation assay. Single frames from time-lapse movies showing maximum overlap between control explants (D), Par3MO-injected explants (E), Par3MO-injected explants in nocodazole (F) and Par3MO-injected explants in NSC23766 (G). Scale bar: 100 μm. (H) Overlap area as a percentage of total explant area (n=23; *P<0.05). (I-L) Cell collision assay. Cell positions were analysed at 15-minute intervals to measure the velocity following collision. Velocity change was clustered in control cells (I; n=10; P<0.001) but no velocity change was observed in Par3MO-injected cells (J; n=10; P<0.005). However, velocity vectors were clustered away from the cell contact in Par3MO-injected cells in nocodazole (K; n=10; P<0.001) and Par3MO-injected cells in NCS23766 (L; n=10; P<0.001). Red arrows indicate the initial velocity vector.

Development (2013) doi:10.1242/dev.098509

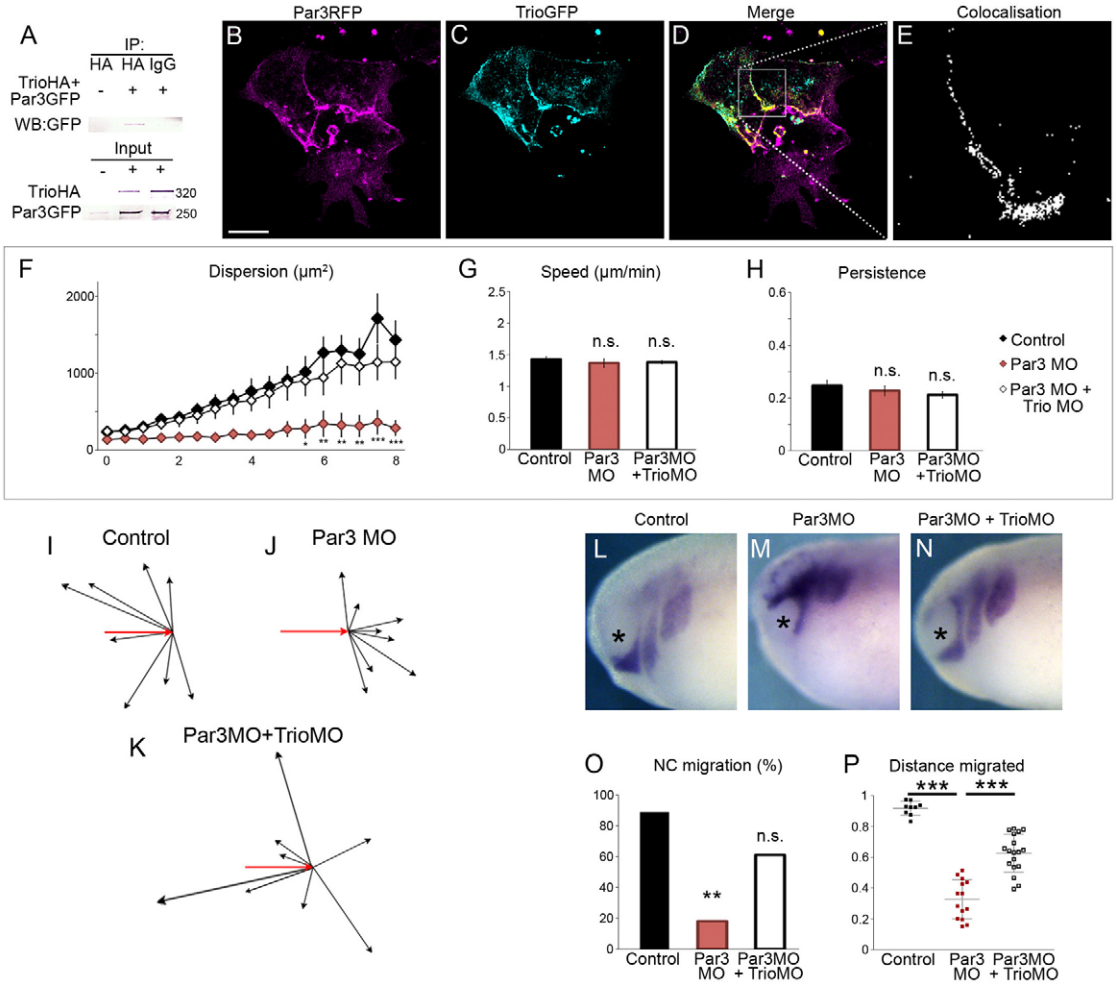

Fig. 9. Trio interacts with Par3 and TrioMO rescues Par3 morphants in *Xenopus*. (A) Co-immunoprecipitation of Trio and Par3 in cells expressing TrioHA and Par3GFP. Following pull-down with the HA tag, western blots against HA showed a band at 320 kDa corresponding to TrioHA and western blots against GFP showed a band at 250 kDa corresponding to Par3GFP. Controls using no transfected cells or control IgG antibody showed no HA or GFP staining. Input lanes show that TrioHA and Par3GFP were present and ran at 320 kDa and 250 kDa, respectively. (B-E) Colocalisation analysis in *Xenopus* NC cells. Par3RFP (B) and TrioGFP (C) are both found at cell-cell contacts, where they colocalise (D). (E) Magnification and colocalisation mask area indicated in D. Scale bar: 20 μm. (F) Dispersion analysis in control (black), Par3MO (red) or Par3Mo/TrioMO (white). n=10 explants for each condition, more than 30 cells analysed per explant; *P<0.05, **P<0.01, ***P<0.001. (G) Speed of migration. Par3MO, n=70; P=0.4642; Par3MO+TrioMO, n=90; P=0.2713. (H) Persistence. Par3MO, n=70; P=0.4637; Par3MO+TrioMO, n=90; P=0.1126. (I-K) Cell collision assay. CIL was analysed with the cell collision assay previously described. (I) Normal CIL behaviour in control cells. n=10; P<0.001. Red arrows indicate the initial velocity vector. (L-P) *Twist* expression in control embryos (L) or those injected with Par3MO (M) or Par3MO+TrioMO (N). Asterisk indicates the eye. (O) Percentage of embryos with normal NC migration. Control, n=9; Par3MO, n=13; **P<0.01; Par3MO+TrioMO, n=18; P<0.05. (P) Distance migrated by NC cells relative to mean migration in control embryos. Migration is reduced in Par3MO-injected embryos (***P<0.001) but co-injection of TrioMO with Par3MO increases migration (***P<0.001). Error bars indicate s.d.

from activating Rac1. This local inhibition of Rac1 activity triggers microtubule catastrophe at the cell-cell contact, resulting in a reversal of cell polarity (Fig. 11C,E), the formation of a new protrusion and a change in the direction of migration, which are typical of contact inhibition behaviour (Fig. 11D). In the absence of Par3, Trio and Rac1 remain active after cell contact, the polymerisation of microtubule continues and cell protrusions do not collapse upon cell contact (Fig. 11F).

Localised microtubule catastrophe leads to an asymmetry in stability across the microtubule array. Work by others has shown that this can result in a change in cellular polarity and migration away from the cell contact as part of a CIL response (Kadir et al., 2011; Stramer et al., 2010). Our results suggest Par3 as a likely candidate to link the cell-cell contact signal to the microtubule catastrophe response in this process.

The Wnt-PCP pathway and N-cadherin are both necessary to reduce Rac1 activity and enhance RhoA activity effectively at the cell-cell contact, as is required to promote CIL (Carmona-Fontaine et al., 2008; Theveneau et al., 2010). Here, we show that Par3 localises to contacts between NC cells, similar to previous findings for epithelial cells (Gao et al., 2002; Izumi et al., 1998; Kuchinke et al., 1998; Suzuki et al., 2001) and wounded fibroblast sheets (Schmoranzer et al., 2009). In contrast to both of these cell types, we find that Par3 neither controls centrosome position (not shown) nor modulates cell-cell adhesion in NC cells. Nonetheless, our results suggest that cell adhesion molecules, such as N-cadherin or cadherin 11, are likely to be regulators of Par3 localisation or activity at the cell contact. This hypothesis is further supported by the fact that N-cadherin-dependent contacts have been shown to affect microtubule organisation and cell polarity in other cell types

Development (2013) doi:10.1242/dev.098509

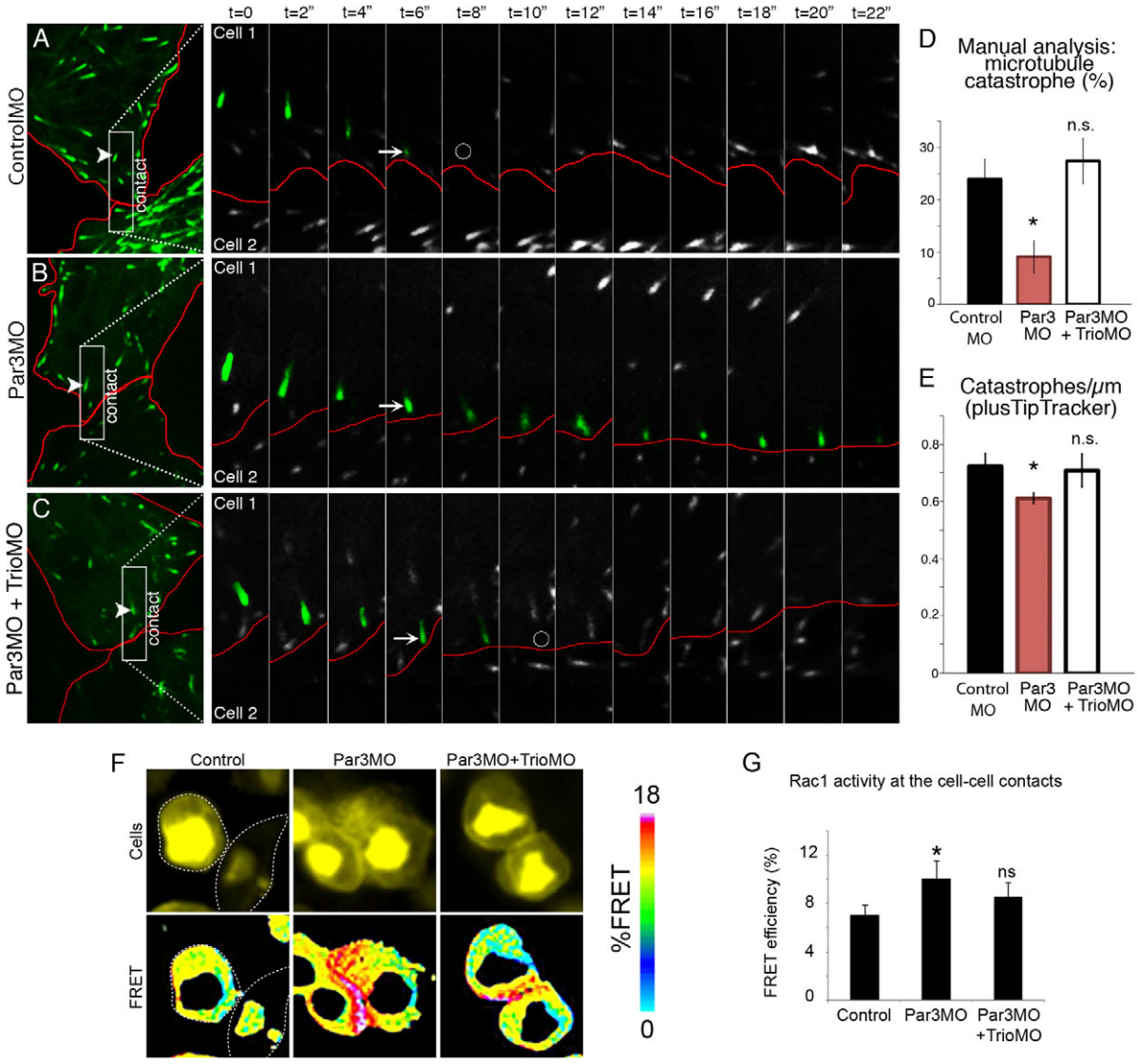

Fig. 10. TrioMO rescues the Par3MO-induced decrease in microtubule catastrophe and increase in Rac activity at contacts in *Xenopus*. (A-D) EB3GFP-labelled cells were manually analysed for microtubule catastrophe. (A-C) ControlMO-injected (A), Par3MO-injected (B) and Par3MO+TrioMO-injected (C) cells undergoing collision; consecutive single frames are presented from time-lapse movies showing one microtubule. The boxed area is shown at higher magnification at the cell-cell contact. Arrowhead indicates the highlighted microtubule. Arrow indicates microtubule in contact with the membrane. Circle indicates site of microtubule collapse. (D) Microtubule catastrophe. Controls versus Par3MO, n=5, *P=0.0258; control versus Par3MO+TrioMO, n=5, P=0.3070. (E) Analysis of EB3GFP-labelled cells using plusTipTracker. *P<0.05. (F,G) FRET analysis of Rac activity in NC. (F) Rac FRET efficiency for control, Par3MO- and Par3MO/TrioMO-injected cells. (G) Rac FRET efficiency at the cell contact. Fifteen cells were analysed per condition from a minimum of four individual explants. *P<0.05. Error bars indicate s.d.

(Camand et al., 2012; Chausovsky et al., 2000; Dupin et al., 2009). Our analysis of cell adhesion molecules and cell sorting does not support the notion that Par3 regulates cell adhesion in NC cells, as has been shown for other cell types (Xue et al., 2013); however, we cannot rule out the possibility that subtle changes in cell adhesion, undetected in our assays, are modulated by Par3 in NC cells. Nonetheless, our data clearly demonstrate a role for Par3 in CIL in NC cells, which could explain some of the phenotypes previously attributed to cell-cell adhesion in other cell types.

Here, we report a novel interaction between Par3 and the Rac-GEF Trio, which could be added to the previously characterised interaction between Par3 and the Rac-GEF Tiam1 at the leading edge and cell-cell contacts (Pegtel et al., 2007). In NC cells, the Rac-GEF Trio has been shown to interact with cadherin 11, which is localised to cell protrusions as well as cell-cell contacts (Kashef et al., 2009). We show that Trio inhibition compensates for a lack of Par3, suggesting that Par3 inhibits Rac-GEF Trio activity at cell-cell contacts during NC migration. RhoA is active at contacts between NC cells (Carmona-Fontaine et al., 2008) and ROCK phosphorylation of Par3 has been shown to disrupt formation of the Par3-aPKC-Par6 complex, through which Par3 often acts (Nakayama et al., 2008). However, ROCK phosphorylation of Par3 does not affect Par3-Tiam2 interactions (Nakayama et al., 2008), suggesting that Par3 is likely to regulate Rac-GEFs independently of its involvement in the Par complex, as has been shown for the regulation of Rac by Par3 in embryonic kidney cells (Mack et al., 2012).

Microtubules are important in the determination and maintenance of cell polarity. Rapid microtubule dynamics allows the microtubule

Development (2013) doi:10.1242/dev.098509

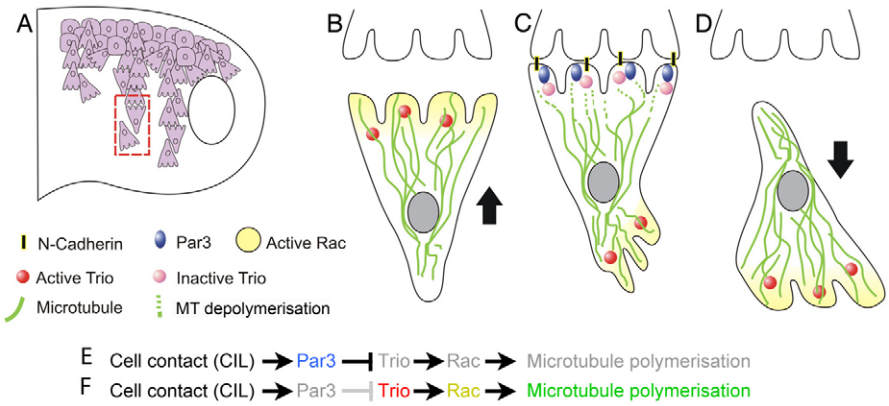

Fig. 11. Par3 controls CIL by inhibiting Trio/Rac and promoting microtubule catastrophe at cell-cell contacts. (A) CIL is required during NC development for directional and collective cell migration. (B) Rac1-Trio activation in the lamellipodia of migrating cells, promoting microtubule stability. (C) Upon contact, Par3 and other proteins such as N-cadherin are localised to the cell-cell contact. Par3 sequestration of Trio at the cell-cell contact to inhibits Rac1-Trio, leading to microtubule catastrophe. Rac1-Trio activation is biased toward another part of the cell, promoting microtubule stability and lamellipodia extension there. (D) The change in Rho-GTPase activity alters cell polarity. A new lamellipodium develops and the cell changes its direction of migration to move away from the contact, completing the process of CIL. (E) Activation of Par3 at the cell contact leads to microtubule depolymerisation. (F) In the absence of Par3, Trio and Rac remain active and microtubule catastrophe is impaired at the cell contact.

array to respond to signals quickly and effectively. Par3 has been shown to stabilise microtubules and promote directional migration at the leading edge of single migrating cells (Pegtel et al., 2007) or during the establishment of neuronal polarity (Chen et al., 2013). However, again illustrating the context-dependent activity of Par3, our data show that Par3 inhibits Rac1 activation at the cell-cell contact to promote microtubule catastrophe. An asymmetry in stability across the microtubule array leads to a change in cell polarity and thus to a change in the direction of migration. In this model, Par3 simply induces a change in direction rather than dictating the direction in which the new protrusion should be extended. As such, it is interesting to note that microtubule depolymerisation, Rac1 inhibition and Trio inhibition – all of which presumably affect the entire cell – are each able to rescue the effect of Par3 inhibition. It is likely that other mechanisms also influence cell-cell contact-induced polarity and that Par3 could have a direct role in microtubule destabilisation. However, our results provide a molecular explanation for the hypothesis put forward by Kadir and colleagues (Kadir et al., 2011) that reaching a threshold of microtubule dynamics at the cell-cell contact is sufficient to induce CIL.

In this study we report a novel interaction between Par3 and the Rac-GEF Trio. We show that Par3 inhibition of Trio at cell-cell contacts promotes microtubule collapse, is required for CIL between NC cells, and is thus essential for the collective and directional migration of NC cells.

MATERIALS AND METHODS

Embryos and microinjections

Xenopus embryos were obtained and staged as described previously (Newport and Kirschner, 1982; Nieuwkoop and Faber, 1994). Embryos were injected at the 8- to 16-cell stage as described (Aybar et al., 2003). Zebrafish strains were maintained and bred according to standard procedures (Westerfield, 2000), injected before division commenced and staged as described (Kimmel et al., 1995). We used two transgenic lines: *sox10:egfp* (Carney et al., 2006) and *sox10:mGFPnRFP* (C.L. and R. Mayor, unpublished). In the latter, the *sox10(4.9)* promoter (Carney et al., 2006) drives NC expression of membrane-bound GFP and nuclear localised RFP separated by the self-cleaving 2A sequence (Stewart et al., 2009).

MOs against *Xenopus Par3* (Par3MO; 8 ng, 3′-TACTTCCACTGC-CACTCGAAACCCT-5′) and *Trio* (TrioMO; 8 ng, 3′-TGCGCATAGCTA-CAGCTGAAAAAAA-5′) were designed by GeneTools. Zebrafish Par3MO has been reported previously [0.21 pmol (Wei et al., 2004)]. Equimolar concentrations of standard control MO (ControlMO) were used in both species. N-cadherinMO was used as described (Theveneau et al., 2010). Fluorescein-dextran (Invitrogen, D1821; 3 µg) or Rhodamine-dextran (Invitrogen, D1824; 5 µg) were used as tracers. Plasmids were linearised and mRNA transcribed as described (Harland and Weintraub, 1985). mRNA constructs injected were: membraneGFP (mbGFP), membraneRFP (mbRFP), EB3GFP (all 300 pg); Par3GFP, Par3RFP (both 500 pg); and p120cateninGFP (120 pg). TrioGFP was injected as DNA (300 pg).

Immunoprecipitation, western blotting, immunostaining and *in situ* hybridisation

Co-immunoprecipitation (Kashef et al., 2009) and western blots (Kuriyama and Mayor, 2009) were performed as described previously using the following antibodies: Par3 (Millipore, 0-330; 1:1000); p42/44 MAPK (Cell Signaling, 9102S; 1:1000); rabbit anti-HA (Abcam; 1:2000); chicken anti-GFP (Abcam; 1:3000); rabbit IgG HRP (ECL, NA934; 1:25,000); rabbit IgG AP (Dianova; 1:2000); chicken IgG AP (Abcam; 1:2000). Band intensity was measured using ImageJ (NIH). *In situ* hybridisation was performed as described (Harland, 1991). NC was labelled with digoxigenin-labelled RNA probes against *Snail2* (Mayor et al., 1995) or *Twist* (Hopwood et al., 1989) in *Xenopus* and *foxd3* in zebrafish (Odenthal and Nüsslein-Volhard, 1998). Cryosectioning was performed using standard procedures. Immunostaining was performed according to standard procedures with α-tubulin (DSHB, 12G10; 1:25), acetylated tubulin (Sigma, 611B1; 1:100), Par3 (1:200), β-catenin (Abcam, ab6302; 1:500), rabbit IgG Alexa 488 (Invitrogen, A11034; 1:100) and mouse IgG Alexa 488 (Invitrogen, A11017; 1:200) antibodies. If required, DAPI was applied with the secondary antibody (Sigma, D9542; 20 µg/ml).

NC manipulation and imaging

Transplants were performed as described (De Calisto et al., 2005). Cranial NC was dissected using a standard technique (Alfandari et al., 2003). Fibronectin dishes were prepared as described (Theveneau et al., 2010) using 10 µg/ml or 50 µg/ml fibronectin (Sigma) for plastic or glass dishes, respectively. When required, nocodazole (Sigma, M1404) or NSC23766 (Tocris, 2161) was added to provide final concentrations of 13 nM and 20 µM, respectively. The cell-sorting assay was performed as described previously (Carmona-Fontaine et al., 2011). Fixed cells or sections were imaged using a Leica SPE confocal microscope. NC explants were observed by low-magnification time-lapse on a Leica DM5500 compound microscope, with frames collected every 5 minutes. High-magnification time-lapse on a spinning disk microscope was used to image individual cells,

with frames collected every 2 seconds. *In vivo* time-lapse of zebrafish NC was performed on a spinning disk microscope, with frames taken every 5 minutes. Pixel intensity was measured using ImageJ.

Cell migration, CIL, microtubule array and FRET analysis

Cells were tracked using the ImageJ Manual Tracking plugin. Track speed and persistence were determined using the ImageJ Chemotaxis Tool plugin. To measure dispersion, the ImageJ Delaunay Triangulation plugin was used. Several methods to study CIL have been developed (Scarpa et al., 2013); we used explant confrontation and cell collision assays as described by Carmona-Fontaine et al. (Carmona-Fontaine et al., 2008). EB3GFP movies were analysed automatically using plusTipTracker (Applegate et al., 2011). The following parameters were used: maximum gap length, 30 frames; minimum track length, 3 frames; search radius range, 5-25 pixels; maximum forward angle, 35°; maximum backward angle, 10°; maximum shrinkage factor, 1.5; fluctuation radius, 2 pixels. For manual analysis, 5×5 µm squares were selected at the front and back of a cell. The total number of $EB3GFP^{+}$ tips that disappeared within the square during a period of 2 minutes was compared with the number that entered the square. Microtubules that were within the square in the final frame were excluded from analysis. All error bars indicate s.e.m. FRET for Rac1 was performed as previously described (Theveneau et al., 2010).

Statistical analysis

Comparison of percentages was performed using contingency tables as described previously (Taillard et al., 2008). Two data sets were considered significantly different (null hypothesis rejected) if $T>3.841$ ($\alpha=0.05$), $T>6.635$ ($\alpha=0.01$) or $T>10.83$ ($\alpha=0.001$). Normality of data sets was tested using Kolmogorov-Smirnov's test, d'Agostino and Pearson's test and Shapiro-Wilk's test using Prism4 (GraphPad). A data set was considered normal if found to be normal by all three tests. Data sets following a normal distribution were compared using Student's *t*-test (two-tailed, unequal variances) or a one-way ANOVA with a Dunnett's multiple comparisons post-test using Excel (Microsoft) or Prism4. Data sets that did not follow a normal distribution were compared using Mann-Whitney's test or a non-parametric ANOVA (Kruskal-Wallis with Dunn's multiple comparisons post-test) using Excel or Prism4. Cross-comparisons were performed only if the overall *P*-value of the ANOVA was less than 0.05.

Acknowledgements

We thank J. Leslie and B. Stramer for comments on the manuscript; and N. Ueno, I. Daar and A. Debant for the EB3, Par3 and Trio fusion proteins, respectively.

Competing interests

The authors declare no competing financial interests.

Author contributions

R. Moore and R. Mayor performed and designed most of the experiments; E.T. helped with statistical analysis and figures; S.P. performed some of the cell-cell adhesion assays; P.A., J.R. and C.L. performed the zebrafish experiments; A.M. and J.K. performed some of the Trio experiments; E.T. and M.P. performed the FRET analysis. The manuscript was written by R. Moore and R. Mayor. All authors commented on the manuscript.

Funding

This study was supported by grants from the Medical Research Council to R. Mayor [MR/J000655/1] and to C.L. J.K. was supported by 'Concept for the Future' of the Karlsruhe Institute of Technology within the framework of the German Excellence Initiative. Deposited in PMC for release after 6 months.

Supplementary material

Supplementary material available online at
http://dev.biologists.org/lookup/suppl/doi:10.1242/dev.098509/-/DC1

References

Abercrombie, M. and Heaysman, J. E. (1953). Observations on the social behaviour of cells in tissue culture. I. Speed of movement of chick heart fibroblasts in relation to their mutual contacts. *Exp. Cell Res.* **5**, 111-131.

Alfandari, D., Cousin, H., Gaultier, A., Hoffstrom, B. G. and DeSimone, D. W. (2003). Integrin alpha5beta1 supports the migration of Xenopus cranial neural crest on fibronectin. *Dev. Biol.* **260**, 449-464.

Applegate, K. T., Besson, S., Matov, A., Bagonis, M. H., Jaqaman, K. and Danuser, G. (2011). plusTipTracker: Quantitative image analysis software for the measurement of microtubule dynamics. *J. Struct. Biol.* **176**, 168-184.

Aybar, M. J., Nieto, M. A. and Mayor, R. (2003). Snail precedes slug in the genetic cascade required for the specification and migration of the Xenopus neural crest. *Development* **130**, 483-494.

Batson, J., Astin, J. W. and Nobes, C. D. (2013). Regulation of contact inhibition of locomotion by Eph-ephrin signalling. *J. Microsc.* **251**, 232-241.

Camand, E., Peglion, F., Osmani, N., Sanson, M. and Etienne-Manneville, S. (2012). N-cadherin expression level modulates integrin-mediated polarity and strongly impacts on the speed and directionality of glial cell migration. *J. Cell Sci.* **125**, 844-857.

Carmona-Fontaine, C., Matthews, H. K., Kuriyama, S., Moreno, M., Dunn, G. A., Parsons, M., Stern, C. D. and Mayor, R. (2008). Contact inhibition of locomotion in vivo controls neural crest directional migration. *Nature* **456**, 957-961.

Carmona-Fontaine, C., Theveneau, E., Tzekou, A., Tada, M., Woods, M., Page, K. M., Parsons, M., Lambris, J. D. and Mayor, R. (2011). Complement fragment C3a controls mutual cell attraction during collective cell migration. *Dev. Cell* **21**, 1026-1037.

Carney, T. J., Dutton, K. A., Greenhill, E., Delfino-Machín, M., Dufourcq, P., Blader, P. and Kelsh, R. N. (2006). A direct role for Sox10 in specification of neural crest-derived sensory neurons. *Development* **133**, 4619-4630.

Chausovsky, A., Bershadsky, A. D. and Borisy, G. G. (2000). Cadherin-mediated regulation of microtubule dynamics. *Nat. Cell Biol.* **2**, 797-804.

Chen, X. and Macara, I. G. (2005). Par-3 controls tight junction assembly through the Rac exchange factor Tiam1. *Nat. Cell Biol.* **7**, 262-269.

Chen, S., Chen, J., Shi, H., Wei, M., Castaneda-Castellanos, D. R., Bultje, R. S., Pei, X., Kriegstein, A. R., Zhang, M. and Shi, S. H. (2013). Regulation of microtubule stability and organization by mammalian Par3 in specifying neuronal polarity. *Dev. Cell* **24**, 26-40.

De Calisto, J., Araya, C., Marchant, L., Riaz, C. F. and Mayor, R. (2005). Essential role of non-canonical Wnt signalling in neural crest migration. *Development* **132**, 2587-2597.

Du, D., Xu, F., Yu, L., Zhang, C., Lu, X., Yuan, H., Huang, Q., Zhang, F., Bao, H., Jia, L. et al. (2010). The tight junction protein, occludin, regulates the directional migration of epithelial cells. *Dev. Cell* **18**, 52-63.

Dupin, I., Camand, E. and Etienne-Manneville, S. (2009). Classical cadherins control nucleus and centrosome position and cell polarity. *J. Cell Biol.* **185**, 779-786.

Friedlander, D. R., Mège, R. M., Cunningham, B. A. and Edelman, G. M. (1989). Cell sorting-out is modulated by both the specificity and amount of different cell adhesion molecules (CAMs) expressed on cell surfaces. *Proc. Natl. Acad. Sci. USA* **86**, 7043-7047.

Gao, L., Macara, I. G. and Joberty, G. (2002). Multiple splice variants of Par3 and of a novel related gene, Par3L, produce proteins with different binding properties. *Gene* **294**, 99-107.

Harland, R. M. (1991). In situ hybridization: an improved whole-mount method for Xenopus embryos. *Methods Cell Biol.* **36**, 685-695.

Harland, R. and Weintraub, H. (1985). Translation of mRNA injected into Xenopus oocytes is specifically inhibited by antisense RNA. *J. Cell Biol.* **101**, 1094-1099.

Hopwood, N. D., Pluck, A. and Gurdon, J. B. (1989). A Xenopus mRNA related to Drosophila twist is expressed in response to induction in the mesoderm and the neural crest. *Cell* **59**, 893-903.

Izumi, Y., Hirose, T., Tamai, Y., Hirai, S. I., Nagashima, Y., Fujimoto, T., Tabuse, Y., Kemphues, K. J. and Ohno, S. (1998). An atypical PKC directly associates and colocalizes at the epithelial tight junction with ASIP, a mammalian homologue of Caenorhabditis elegans polarity protein PAR-3. *J. Cell Biol.* **143**, 95-106.

Kadir, S., Astin, J. W., Tahtamouni, L., Martin, P. and Nobes, C. D. (2011). Microtubule remodelling is required for the front-rear polarity switch during contact inhibition of locomotion. *J. Cell Sci.* **124**, 2642-2653.

Kashef, J., Köhler, A., Kuriyama, S., Alfandari, D., Mayor, R. and Wedlich, D. (2009). Cadherin-11 regulates protrusive activity in Xenopus cranial neural crest cells upstream of Trio and the small GTPases. *Genes Dev.* **23**, 1393-1398.

Kimmel, C. B., Ballard, W. W., Kimmel, S. R., Ullmann, B. and Schilling, T. F. (1995). Stages of embryonic development of the zebrafish. *Dev. Dyn.* **203**, 253-310.

Kuchinke, U., Grawe, F. and Knust, E. (1998). Control of spindle orientation in Drosophila by the Par-3-related PDZ-domain protein Bazooka. *Curr. Biol.* **8**, 1357-1365.

Kuriyama, S. and Mayor, R. (2009). A role for Syndecan-4 in neural induction involving ERK- and PKC-dependent pathways. *Development* **136**, 575-584.

Mack, N. A., Porter, A. P., Whalley, H. J., Schwarz, J. P., Jones, R. C., Khaja, A. S., Bjartell, A., Anderson, K. I. and Malliri, A. (2012). β2-syntrophin and Par-3 promote an apicobasal Rac activity gradient at cell-cell junctions by differentially regulating Tiam1 activity. *Nat. Cell Biol.* **14**, 1169-1180.

Matthews, H. K., Marchant, L., Carmona-Fontaine, C., Kuriyama, S., Larraín, J., Holt, M. R., Parsons, M. and Mayor, R. (2008). Directional migration of neural crest cells in vivo is regulated by Syndecan-4/Rac1 and non-canonical Wnt signaling/RhoA. *Development* **135**, 1771-1780.

Mayor, R. and Carmona-Fontaine, C. (2010). Keeping in touch with contact inhibition of locomotion. *Trends Cell Biol.* **20**, 319-328.

Mayor, R., Morgan, R. and Sargent, M. G. (1995). Induction of the prospective neural crest of Xenopus. *Development* **121**, 767-777.

Mertens, A. E., Rygiel, T. P., Olivo, C., van der Kammen, R. and Collard, J. G. (2005). The Rac activator Tiam1 controls tight junction biogenesis in keratinocytes

through binding to and activation of the Par polarity complex. *J. Cell Biol.* **170**, 1029-1037.
Mishima, A., Suzuki, A., Enaka, M., Hirose, T., Mizuno, K., Ohnishi, T., Mohri, H., Ishigatsubo, Y. and Ohno, S. (2002). Over-expression of PAR-3 suppresses contact-mediated inhibition of cell migration in MDCK cells. *Genes Cells* **7**, 581-596.
Nakayama, M., Goto, T. M., Sugimoto, M., Nishimura, T., Shinagawa, T., Ohno, S., Amano, M. and Kaibuchi, K. (2008). Rho-kinase phosphorylates PAR-3 and disrupts PAR complex formation. *Dev. Cell* **14**, 205-215.
Newport, J. and Kirschner, M. (1982). A major developmental transition in early Xenopus embryos: I. characterization and timing of cellular changes at the midblastula stage. *Cell* **30**, 675-686.
Nieuwkoop, P. D. and Faber, J. (1994). *Normal Table of Xenopus laevis (Daudin)*. Amsterdam: North Holland Publishing.
Nishimura, T., Yamaguchi, T., Kato, K., Yoshizawa, M., Nabeshima, Y. I., Ohno, S., Hoshino, M. and Kaibuchi, K. (2005). PAR-6-PAR-3 mediates Cdc42-induced Rac activation through the Rac GEFs STEF/Tiam1. *Nat. Cell Biol.* **7**, 270-277.
Odenthal, J. and Nüsslein-Volhard, C. (1998). fork head domain genes in zebrafish. *Dev. Genes Evol.* **208**, 245-258.
Pegtel, D. M., Ellenbroek, S. I. J., Mertens, A. E. E., van der Kammen, R. A., de Rooij, J. and Collard, J. G. (2007). The Par-Tiam1 complex controls persistent migration by stabilizing microtubule-dependent front-rear polarity. *Curr. Biol.* **17**, 1623-1634.
Scarpa, E., Roycroft, A., Theveneau, E., Terriac, E., Piel, M. and Mayor, R. (2013). A novel method to study contact inhibition of locomotion using micropatterned substrates. *Biol. Open* **2**, 901-906.
Schmoranzer, J., Fawcett, J. P., Segura, M., Tan, S., Vallee, R. B., Pawson, T. and Gundersen, G. G. (2009). Par3 and dynein associate to regulate local microtubule dynamics and centrosome orientation during migration. *Curr. Biol.* **19**, 1065-1074.
Shin, K., Wang, Q. and Margolis, B. (2007). PATJ regulates directional migration of mammalian epithelial cells. *EMBO Rep.* **8**, 158-164.
Stewart, M. D., Jang, C. W., Hong, N. W., Austin, A. P. and Behringer, R. R. (2009). Dual fluorescent protein reporters for studying cell behaviors in vivo. *Genesis* **47**, 708-717.
Stramer, B., Moreira, S., Millard, T., Evans, I., Huang, C. Y., Sabet, O., Milner, M., Dunn, G., Martin, P. and Wood, W. (2010). Clasp-mediated microtubule bundling regulates persistent motility and contact repulsion in Drosophila macrophages in vivo. *J. Cell Biol.* **189**, 681-689.
Stramer, B. M., Dunn, G. A., Davis, J. R. and Mayor, R. (2013). Rediscovering contact inhibition in the embryo. *J. Microsc.* **251**, 206-211.
Suzuki, A., Yamanaka, T., Hirose, T., Manabe, N., Mizuno, K., Shimizu, M., Akimoto, K., Izumi, Y., Ohnishi, T. and Ohno, S. (2001). Atypical protein kinase C is involved in the evolutionarily conserved par protein complex and plays a critical role in establishing epithelia-specific junctional structures. *J. Cell Biol.* **152**, 1183-1196.
Taillard, E. D., Waelti, P. and Zuber, J. (2008). Few statistical tests for proportions comparison. *Eur. J. Oper. Res.* **185**, 1336-1350.
Theveneau, E. and Mayor, R. (2011). Collective cell migration of the cephalic neural crest: the art of integrating information. *Genesis* **49**, 164-176.
Theveneau, E. and Mayor, R. (2012). Cadherins in collective cell migration of mesenchymal cells. *Curr. Opin. Cell Biol.* **24**, 677-684.
Theveneau, E., Marchant, L., Kuriyama, S., Gull, M., Moepps, B., Parsons, M. and Mayor, R. (2010). Collective chemotaxis requires contact-dependent cell polarity. *Dev. Cell* **19**, 39-53.
Theveneau, E., Steventon, B., Scarpa, E., Garcia, S., Trepat, X., Streit, A. and Mayor, R. (2013). Chase-and-run between adjacent cell populations promotes directional collective migration. *Nat. Cell Biol.* **15**, 763-772.
Wei, X., Cheng, Y., Luo, Y., Shi, X., Nelson, S. and Hyde, D. R. (2004). The zebrafish Pard3 ortholog is required for separation of the eye fields and retinal lamination. *Dev. Biol.* **269**, 286-301.
Westerfield, M. (2000). *The Zebrafish Book. A Guide for the Laboratory Use of Zebrafish (Dario rerio)*. Eugene, OR: University of Oregon Press.
Wittmann, T., Bokoch, G. M. and Waterman-Storer, C. M. (2003). Regulation of leading edge microtubule and actin dynamics downstream of Rac1. *J. Cell Biol.* **161**, 845-851.
Xue, B., Krishnamurthy, K., Allred, D. C. and Muthuswamy, S. K. (2013). Loss of Par3 promotes breast cancer metastasis by compromising cell-cell cohesion. *Nat. Cell Biol.* **15**, 189-200.

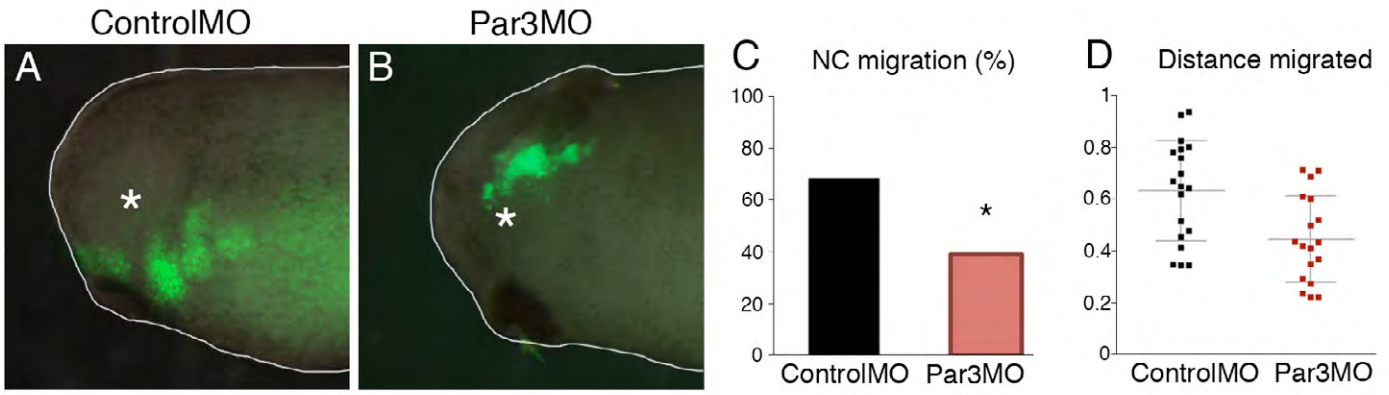

Fig. S1. Par3 is required in neural crest cells. (A-B) Grafts of fluorescently labelled NC cells into control host embryos. NC were injected with controlMO (A) or Par3MO (B). (C) Percentage of embryos with migratory grafted NC cells. Par3MO, n=18; ControlMO, n=19; $p<0.05$. (D) Average distance of NC migration for each grafted embryo. ControlMO, n=19; Par3MO, n=18; $p=0.0035$, error bars show mean and s.d.

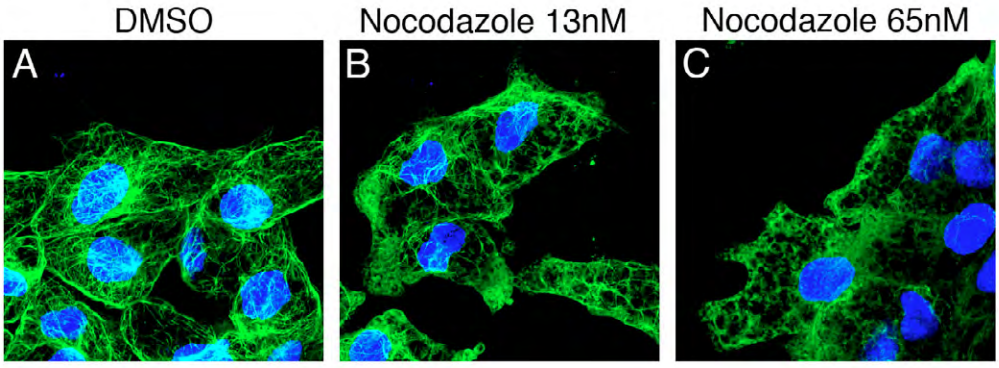

Fig. S2. Effect of nocodazole on microtubule array in NC cells. (A-C) Immunostaining against αtubulin shows the microtubule array in control NC cells (A) or NC cells treated with 13nM (B) or 65nM (C) of nocodazole. Note that in cells treated with the nocodazole concentration used to rescue Par3MO (13nM, panel B) microtubules are not completely depolymerized.

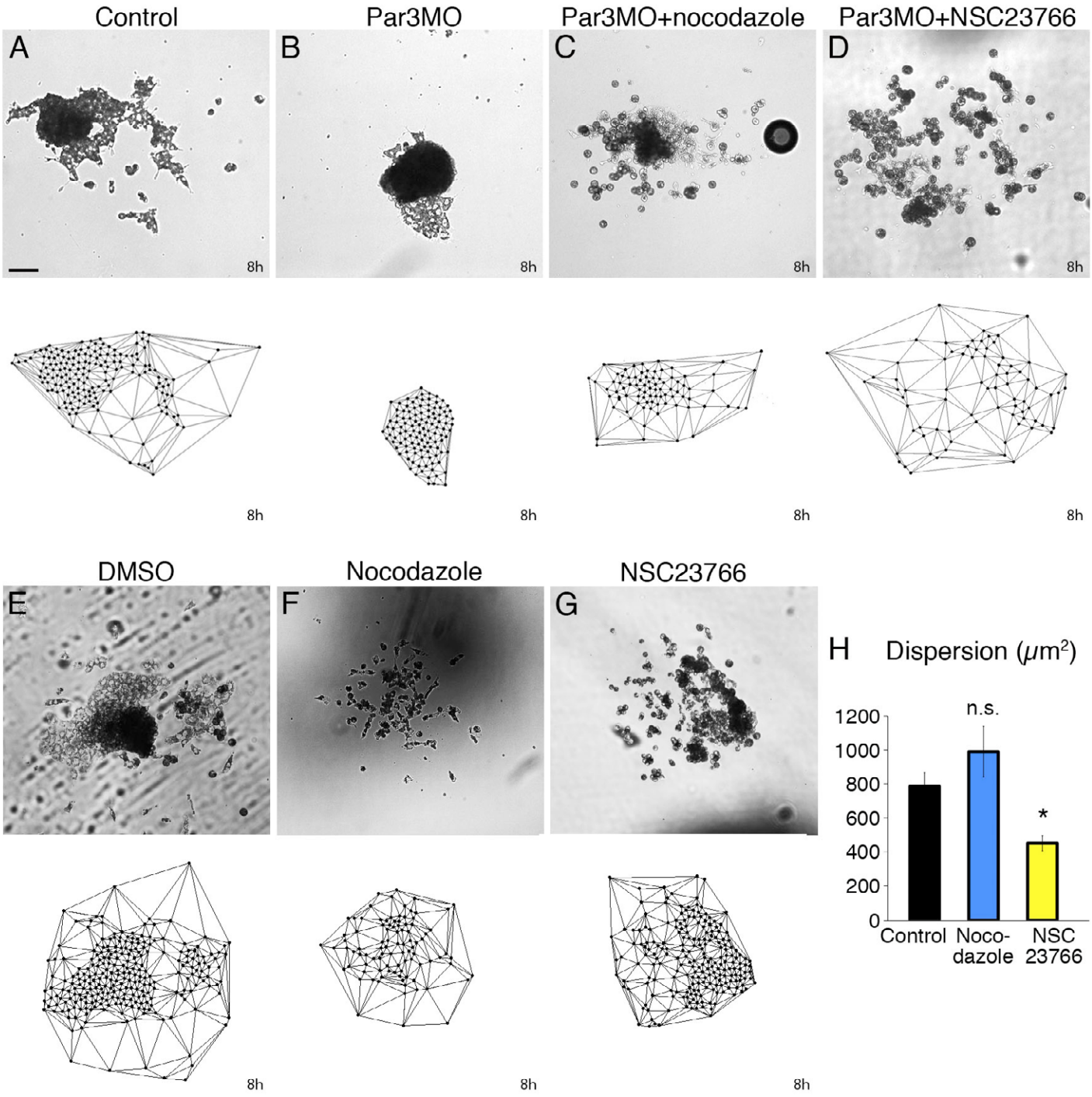

Fig. S3. Nocodazole and NSC23766 can restore normal dispersion in Par3MO NC cells. (A-D) Dispersion assay in control NC cells (A), Par3MO NC cells (B), Par3MO NC cells treated with nocodazole (C) and Par3MO NC cells treated with Rac inhibitor NSC23766 (D). (E-G) Dispersion assay in control NC cells (E), control NC cells treated with nocodazole (F) and control NC cells treated with Rac inhibitor NSC23766 (G). Note that nocodazole alone does not have an effect on NC dispersion. (H) Quantification of NC dispersion from the experiment depicted in E-G.

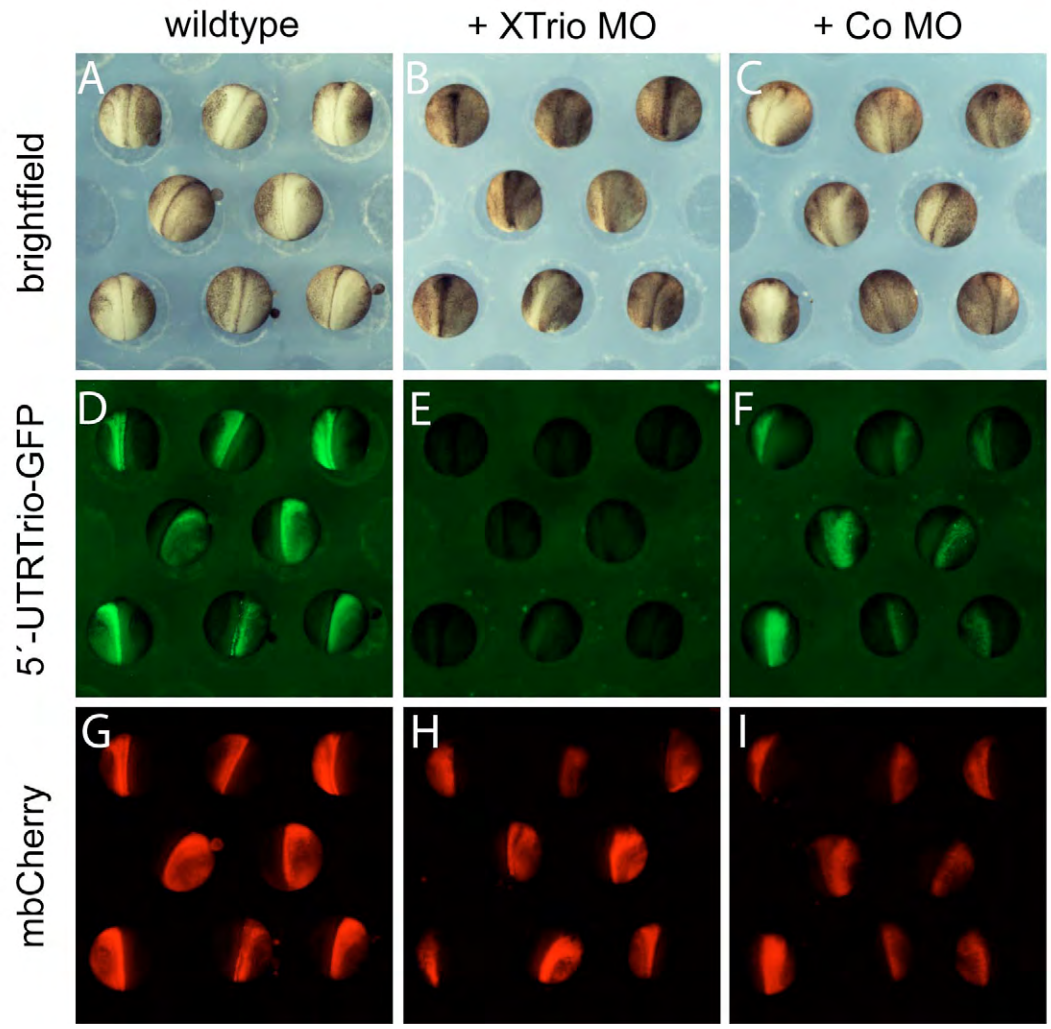

Fig. S4. Efficiency of Trio MO. Embryos were injected unilaterally with 5'UTRTrio-GFP and membraneCherry mRNA (A, D, G), together with TrioMO (B, E, H) or a control MO (C, F, I). Pictures are shown for bright field (A-C), GFP (D-F) or RFP (G-I) fluorescence. Note that injection of Trio MO leads to a strong inhibition of GFP fluorescence, indicating an efficient decrease of Trio-GFP protein.

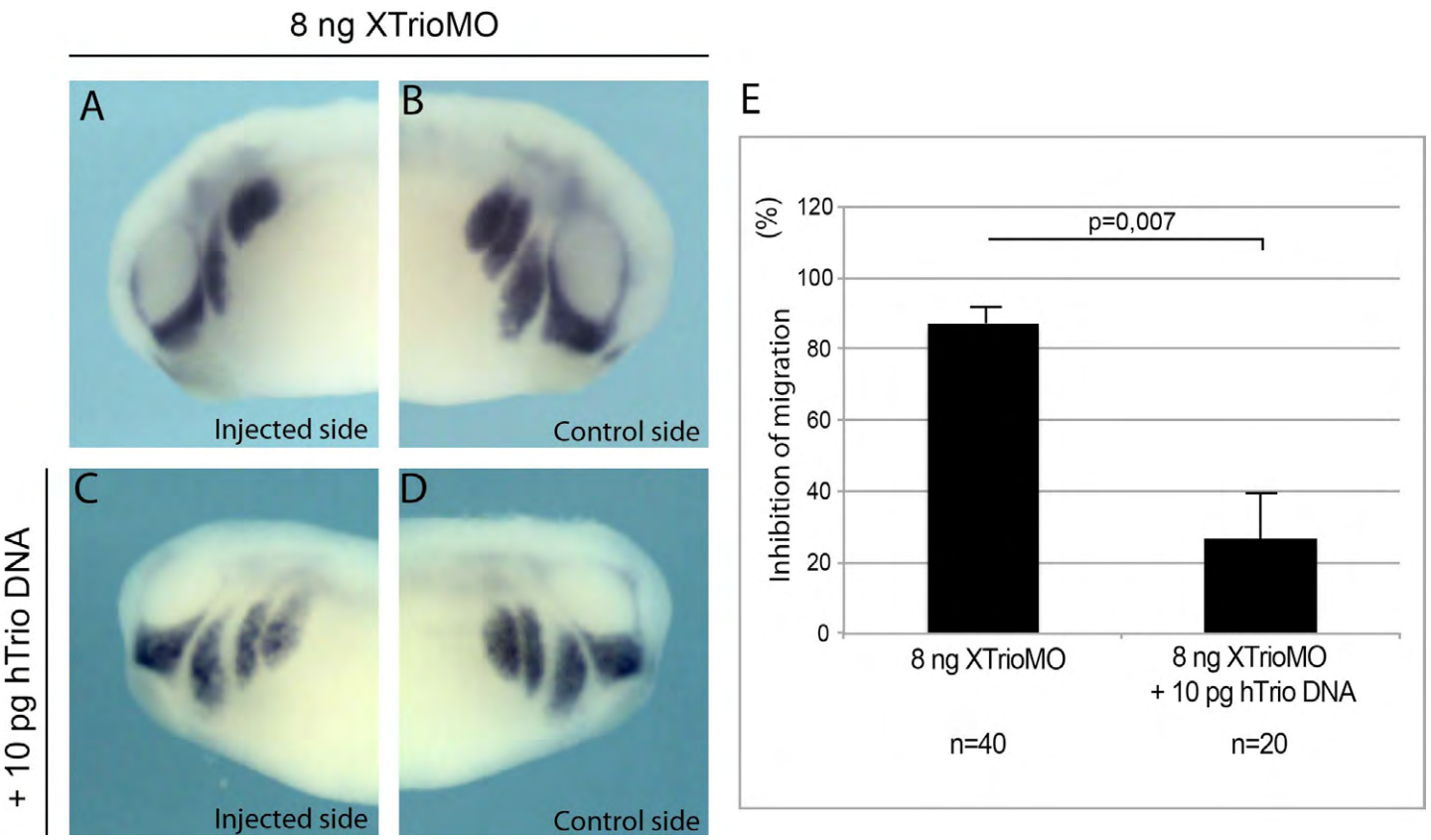

Fig. S5. Specificity of Trio MO. Embryos were injected at the two cell stage as indicated, fixed at stage 25 and migration of neural crest cells was analysed by in situ hybridization against Xtwist. (A, B) Injection of TrioMO leads to a clear inhibition of neural crest migration at the injected side. (C, D) This inhibition of neural crest migration was rescued by co-injection of human Trio that is not recognized by Trio MO. (E) Quantification of inhibition in neural crest migration produced by TrioMO and its rescue by co-injection of human Trio DNA. This efficient rescue of TrioMO by Trio DNA shows the specificity of Xenopus TrioMO used in this work.

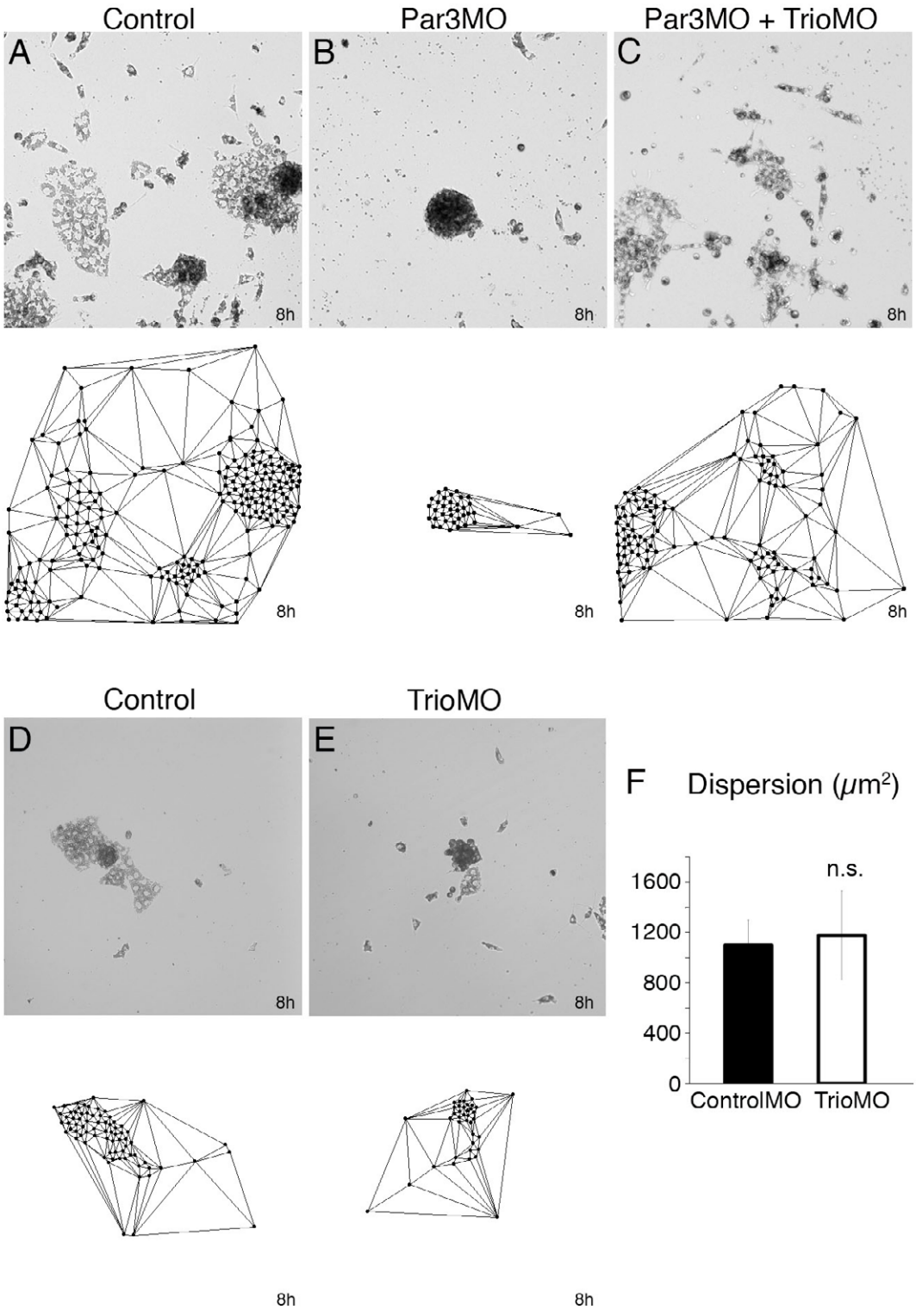

Fig. S6. Trio inhibition can restore normal dispersion in Par3MO cells. (A-D) Dispersion assay in control NC cells (A), Par3MO NC cells (B), Par3MO NC cells co-injected with TrioMO (C). (D-E) Dispersion assay in control NC cells (D) and TrioMO NC cells (E). Note that inhibition of Trio alone does not affect NC dispersion. (F) Quantification of NC dispersion from the experiment depicted in D-E.

Movie 1. Neural crest cell migration assay with control cells (left panel) and cells injected with Par3MO. Note that Par3MO-injected cells fail to disperse. 10X Objective, 1 picture / 5 minutes, 8 hours.

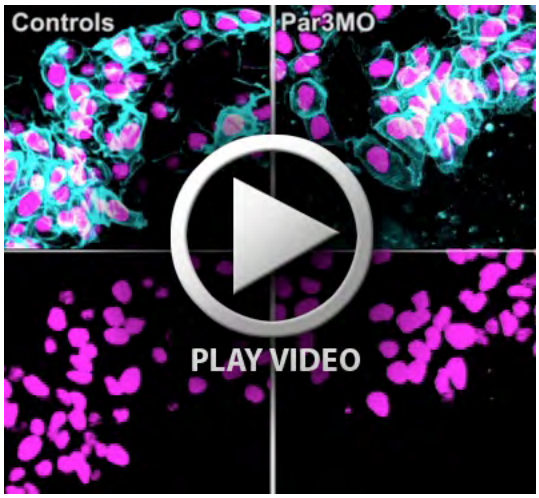

Movie 2. In vivo time-lapse movie of zebrafish neural crest cells. Control cells (left panels), Par3MO-injected cells (right panels). Note that Par3MO cells fail to disperse. Confocal spinning disk microscope 40 objective, 1 picture / X minutes, X hours.

Movie 3. Control (upper panel) and Par3MO-injected (lower panel) neural crest cells expressing membrane-GFP. Note that Par3MO cells tend to overlap with one another. 63X Objective, 1 picture / 30 seconds, 30 minutes.

Movie 4. Collision assay with control (left panel) and Par3MO-injected (right panel) neural crest cells. 10X Objective, 1 picture / 5 minutes, 45 minutes.

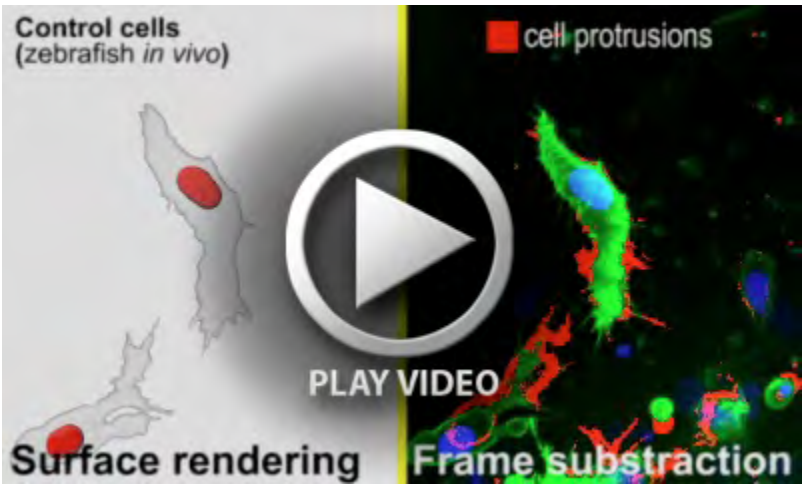

Movie 5. In vivo time-lapse movie of zebrafish neural crest cells. Collision between two control neural crest cells. Left panel shows surface rendering and tracks of the colliding cells. Right panel shows the substraction of consecutive frames in which growing membranes (protrusions) are colour-coded in red. 40 objective, 1 picture / 10 minutes, X minutes.

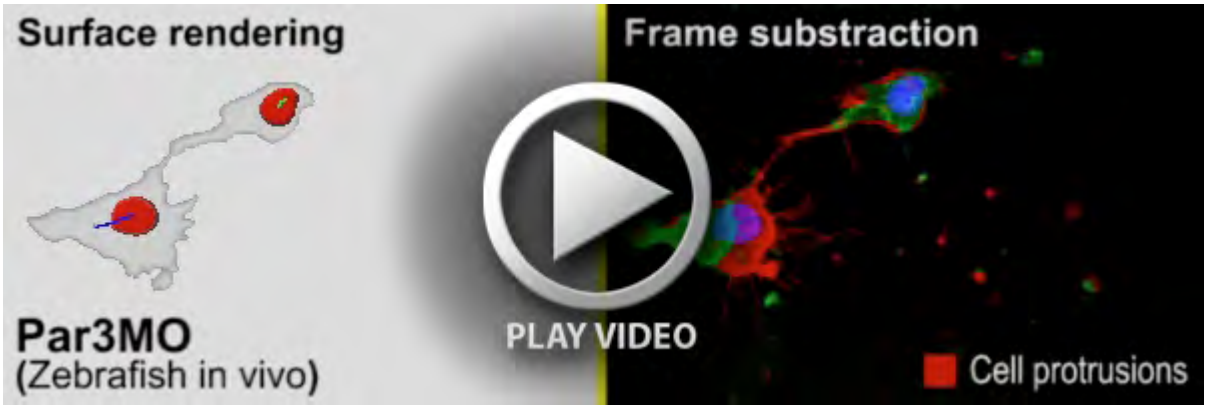

Movie 6. In vivo time-lapse movie of zebrafish neural crest cells. Collision between two Par3MO-injected neural crest cells. Left panel shows surface rendering and tracks of the colliding cells. Right panel shows the substraction of consecutive frames in which growing membranes (protrusions) are colour-coded in red. 40 objective, 1 picture / 5 minutes, X minutes.

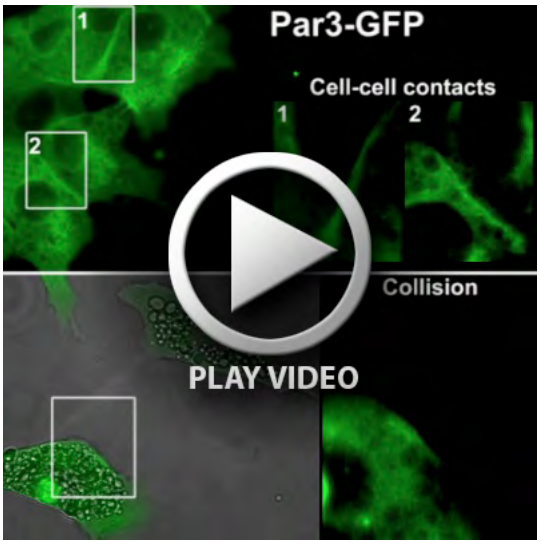

Movie 7. In vitro time-lapse movie with control neural crest cells overexpressing Par3-GFP. Par3 is seen at cell-cell junctions in cells that are in direct apposition (upper panel) and accumulating at the cell-cell contact in colliding cells (lower panel). 63X Objective, 1 picture / 1 minute, 15 minutes.

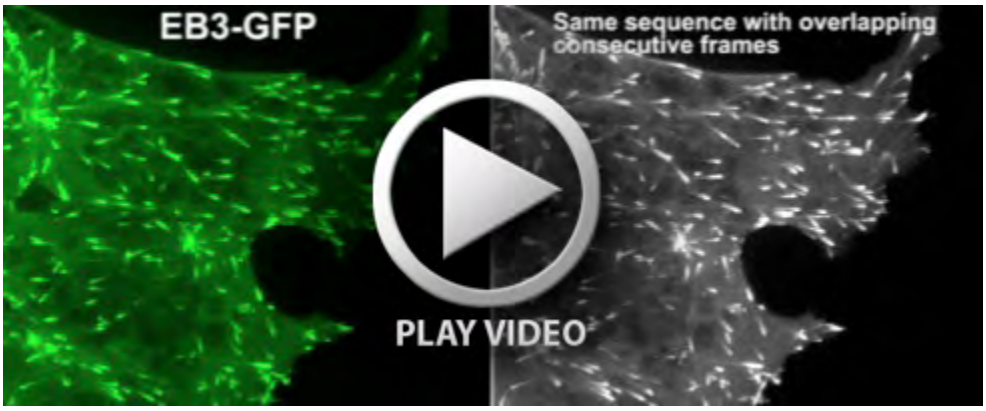

Movie 8. In vitro time-lapse movie with control neural crest cells overexpressing EB3-GFP. Left panel shows EB3-GFP. Right panel shows the same sequence with overlapping consecutive frames to make microtubule trajectories more evident. 63X Objective, 1 picture / 6 seconds, 7.8 minutes.

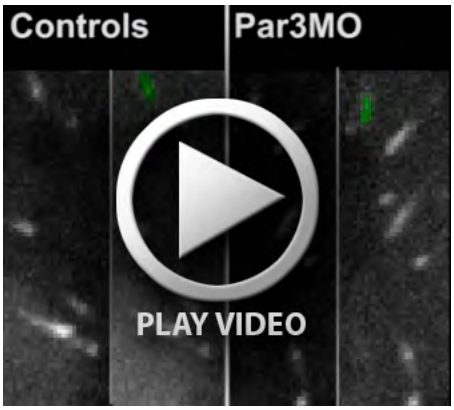

Movie 9. Examples of microtubule tips labelled with EB3-GFP arriving at the region of cell-cell contact in control Neural crest cells (left panel) or Par3MO-injected neural crest cells. 63X Objective, 1 picture / 2 seconds, 36 seconds.

Movie 10. Neural crest cell migration assay with control cells (top left panel), cells injected with Par3MO (top right panel) or cells injected with Par3MO and treated with nocodazole (bottom left panel) or Rac1 inhibitor (NSC 23766, bottom right panel). 10X Objective, 1 picture / 7 minutes, 8 hours.

Movie 11. Collision assay with control cells (top left panel), cells injected with Par3MO (top right panel) or cells injected with Par3MO and treated with nocodazole (bottom left panel) or Rac1 inhibitor (NSC 23766, bottom right panel). 10X Objective, 1 picture / 5 minutes, 50 minutes.

Movie 12. Neural crest cell migration assay with control cells (left panel), cells injected with Par3MO (middle panel) or cells co-injected with Par3MO and TrioMO (right panel). 10X Objective, 1 picture / 5 minutes, 8 hours.

Movie 13. Collision assay with control neural crest cells (left panel), cells injected with Par3MO (middle panel) or cells co-injected with Par3MO and TrioMO (right panel). 10X Objective, 1 picture / 7 minutes, 49 minutes.